Ice Storage Model-Predictive Control in an Office Building with PV: Scenario, Error and Sensitivity Analysis

Darice Guittet*[1], Eric Bonnema[1], Matt Mitchell[1], Allison Mahvi[2], and Jason Woods[1]

[1]National Renewable Energy Laboratory, Golden, CO 80401, USA
[2]University of Wisconsin, Madison, WI 53706, USA
*Correspondence: darice.guittet@nrel.gov

Abstract

Thermal energy storage (TES) can enable more building-sited renewable electricity generation and lower utility bill costs for buildings owners and occupants, especially when there are high demand and variable time-of-use (TOU) charges. A model predictive control (MPC) strategy can offer additional savings over a schedule-based control with added complexity and reliance on forecasts. This study examines savings for medium office buildings with chiller plants in three locations with building-installed solar photovoltaics (PV) to understand the impact of MPC. Control setpoints are fixed by a schedule-based control or optimized by nonlinear MPC. These control setpoints are actuated within EnergyPlus building models to simulate the utility cost of the chiller plant. NLP solutions can be unstable or unrealistic, but our results show that by regularizing the NLP, the solutions can be reasonably followed by the building model. MPC models make simplifications that lead to errors once the controller is participating in and changing the operation of the building. These errors average 9% across the cases, showing that the most important parts of the system are represented. The no-thermal load costs are computed to show that the optimization can in some cases achieve both the minimum TOU and minimum monthly demand costs by demand management while reducing TOU energy costs by energy arbitrage. The MPC saves 35-66% in the annual chiller plant operating costs, which is an additional savings above the schedule by 1-33%. PV and TES are complementary and mostly independent, but a load with PV often results in better performance for the schedule. Our case study and sensitivity analysis show the importance of modeling and optimization for complex rates, but also the circumstances wherein a simpler strategy achieves the same performance with less potential for error.

Keywords— thermal energy storage, nonlinear model predictive control, ice tank, demand management, utility cost minimization, optimal control

1 Introduction

Energy storage is becoming increasingly important to enable a clean and reliable electricity grid [1]. Much of the demand on the electric grid is from buildings, and in many climates air conditioning in buildings drives the peak demand on the grid, with electric generators built solely to support this cooling load on the hottest days of the year. Behind-the-meter thermal energy storage (TES) can provide much of the storage capacity needed [2, 3], decoupling the time when heating and cooling equipment use electricity from the time when this equipment provides heating or cooling to the building, making it an attractive option to

reduce the mismatch between supply and demand. This storage resource would increase the opportunity for more building-sited renewable electricity generation and lower electricity costs for building owners and occupants.

TES has been in use for several decades to reduce a building's cooling demand during peak periods and the corresponding utility cost. In addition to time-of-use (TOU) energy rates that change with the hour of day and/or month of year, some utilities impose TOU demand and monthly demand charges. TOU demand charges also vary with the hour of day and/or month of year, but the charge is applied to the peak demand occurring within a predefined period of time. Similarly, monthly demand charges are applied to the peak demand occurring within the month. There has been extensive work on TES optimal control for utility bill cost reduction, with a variety of modeling approaches, optimization algorithms, combinations of utility bill components, and co-sited technologies.

Ice storage traditionally has been used by creating ice at night and melting ice during the day with relatively simple schedule-based and heuristic control strategies. This includes full-load shifting, where the storage is large enough such that the chiller is completely off during the peak period. It also includes partial-load shifting methods, which can be either chiller-priority or TES-priority [4]. In the chiller-priority method, the chiller operates at a nominal capacity and the TES meets the remaining load. In the TES-priority method, it is reversed—the TES is fully discharged during the peak period, and the chiller provides supplemental cooling.

Drees and Braun evaluated a near-optimal control strategy against chiller-priority and storage-priority control, for which the costs were as much as 20% or 6%, respectively, greater than that of the optimal control [5]. Al-Aali et al. determined optimal equipment scheduling and dispatch of a chilled-water plant with ice storage for a TOU energy rate and found that the optimal strategy reduced costs by $\sim$20% relative to the chiller-priority control and $\sim$12% compared to the storage-priority control [6]. These increased to 26% and 17%, respectively, when including a $20/kW constant demand charge. Chen et al. determined the optimal dispatch for a chiller plant with ice storage where the cost of cooling delivery varies within a factor of three over different periods during the day [7]. They found that a genetic algorithm-based optimal control strategy reduced electricity consumption by 7% and operating costs by approximately 9%. Kang et al. investigated different algorithms for predicting cooling load, including one where the prediction was updated once per day and another updated five times per day [8].

Buildings with on-site solar photovoltaic (PV) generation can offset much of the building load during the day. Electric utilities in locations with high PV penetration are shifting their highest demand-charge periods and highest TOU electricity rates to later in the day, when PV generation drops [9]. Complex rate structures with larger energy and demand charge ratios require more sophisticated ice tank controls and have the potential for greater savings while being more sensitive to errors in optimization. Using dynamic programming to ensure global optimality for the non-linear programming (NLP) problem, Hao et al. co-optimized a UA-based TES model or battery storage with PV and a chiller for rates including anytime or off-peak demand charges [10]. Saffari et al. optimized with constraint programming an industrial TES with PV system under rates with TOU energy and TOU demand charges and found that PV mostly reduced energy costs, TES mostly demand, and coupled together, they led to higher utility cost reductions compared to separately [11].

However, none of these studies have looked at rates where there are both TOU demand and monthly/anytime demand. A large monthly demand rate will incentivize flattening the total load over all periods whereas a large TOU demand/energy rate will incentivize shifting the total load out of the most expensive periods into the cheapest periods. The control optimization must make trade-offs between the two types of demand costs, in addition to energy cost. Controlling monthly demand often requires flattening the total load for a longer duration, which requires very dynamic chiller control and can be quite sensitive to control and forecast errors.

Some papers consider integration of strategies into building control systems by generating reduced-order or heuristic control algorithms based on full optimization results [5], [12]. For a packaged chiller unit

integrated with TES, Tam et al. evaluates an optimal controller against a rule-based controller trained on results from the optimal controller that can handle anytime or off-peak demand charges, studying 6 types of rates to find that the rule-based controller was within 20% of the optimal [12]. The uncertainty and complexity of the control environment can be addressed by reinforcement learning (RL)-based methods, which allow for faster decision-making after the time- and computation-intensive training stage is complete. Wang et al. compared the performance of a chiller and TES plant under a TOU tariff and cooling load uncertainty using RL control, a fixed schedule, a rule-based control and a no-uncertainty rule-based control, the latter of which serves as an "ideal case" against which the RL model is compared [13]. The unstable training process and unpredictable convergence of the model make it difficult to achieve optimal control, and like with NLP, there is no direct way to measure how far the solution is from the global optimum.

Studies of MPC performance when operating in a physical building should be considered in future work. Accurate forecasts and building component models will be critical to the performance of control actions on the entire building [14]. While studies have investigated the impact of uncertainty and forecasting on control performance, there has been no study on control and optimization errors when an MPC is operated in a full-building simulation.

This study presents a detailed case study of the impact of an NLP-based MPC compared with a traditional, no-forecasting schedule-based control for ice TES across three different utility rate structures and climates, on buildings with and without rooftop PV. Our novel contribution consists of 2 parts:

1. Utility rates that include TOU energy with simultaneous TOU demand and monthly/anytime demand charges
2. Performance gap analysis between the algorithms' predicted results to simulated results produced by implementing control actions within a full building simulation

The simulation environment is EnergyPlus®, into which an experiment-informed ice tank TES model designed to simulate variable heat transfer rates was integrated within a building model using the Python plugin [15]. The optimization model is a separate process than that of the EnergyPlus simulation, representing the most salient features of the TES, the chiller plant, and the rest of the building as a NLP. Even with nearly-perfect load forecasting (weather or load uncertainty are not examined in our study), it still contains simplifications that can lead to errors once the MPC controller is actively participating in and changing the operation of the complex building model. The NLP's optimality is estimated by its distance from the no-thermal load cost, showing how the solver can achieve the global minimum demand (monthly and TOU) in some cases. The optimized loads, utility cost components and errors of the MPC and the schedule-based control strategy are evaluated, with a brief sensitivity analysis of annual costs to climate and utility rate.

2 Methods

This section describes the experiment-informed ice tank model and the approach for estimating the impact of control strategy on utility bill costs for the three scenarios. The simulation consists of three main steps: baseline simulations, mathematical optimization of the MPC, and ice tank simulations using the schedule control and the MPC building models. The approach is summarized in Figure 1.

There are four cases examined in this study—base, schedule, optimal, and MPC. The base, schedule, and MPC cases are each run using a dedicated EnergyPlus building model, described in Section 2.2. The integration of the ice tank model and implementation of setpoint control within the schedule-control and MPC building models are described in Section 2.5.

- Base: The base building model provides the business-as-usual utility cost for comparison with adding

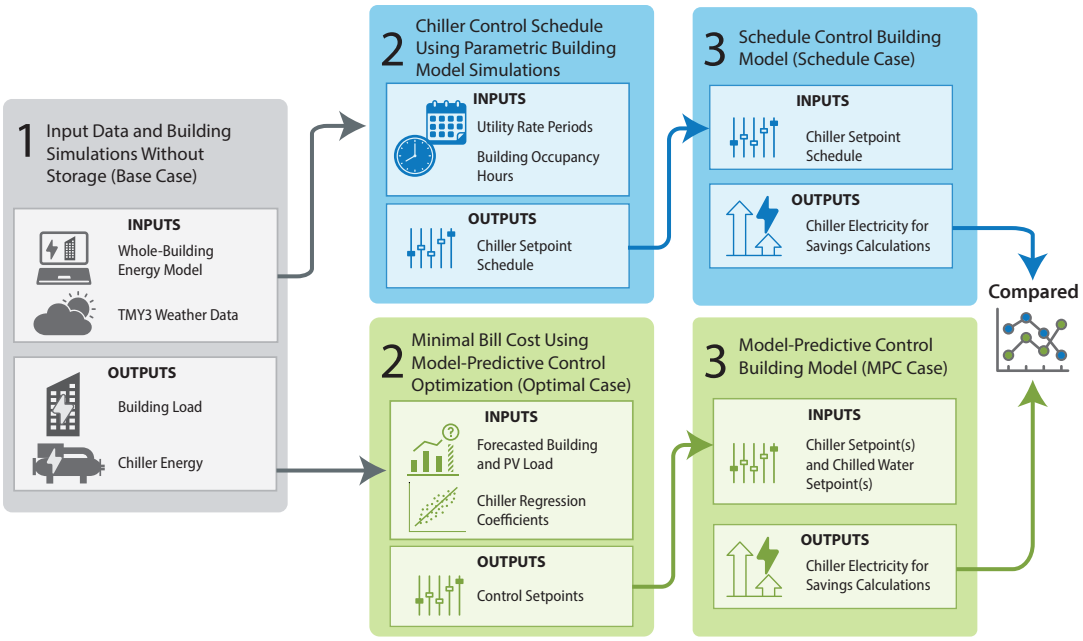

Figure 1: Simulation approach for estimating the impact of ice storage control strategy
Figure by Marjorie Schott, NREL

TES and is used to generate data for the MPC.

- Schedule: The schedule-control building model modifies the chiller setpoints according to a chiller control schedule decided by a one-time parametric sizing process determined using utility rate peak pricing windows, described in Section 2.4.1.
- Optimal: This case is the control strategy predicted to be optimal by the non-linear optimization problem described in Section 2.4.2, but has not yet been run in the MPC building model.
- MPC: The MPC building model implements the control strategy of the Optimal case by modifying chiller and chilled water setpoints to verify the predicted performance of the Optimal case.

2.1 Experiment-Informed Ice Tank Model

The existing ice storage tank models incorporated into EnergyPlus were found to be inadequate for this application during validation with the experimental ice tank data collected. A flexible Python-based model that can be used through the EnergyPlus Python plugin system was developed and calibrated to the experimental data.

2.1.1 Ice Tank Model

The ice tank model is an effectiveness-NTU ("number of transfer units") model that assumes that the heat storage media behaves as a lumped capacitance, based on semi-empirical model developed in [16] and similar to the model used in [17], [10] and [12]. An energy balance evaluates the new state of charge (SOC) of the storage media. The general governing equation, Equation 1, is solved at each simulation timestep.

$$M_f du = Q_{env} + Q_{glycol} \tag{1}$$

where M_f is the mass of the storage media in kg; du is the change in internal energy of the storage media in $\mathrm{J/kg}$; Q_{env} is the energy transfer between the environment and the storage media in J, and Q_{glycol} is the energy transfer between the circulating glycol and the storage media in J. To solve Equation 1, the right-hand side is evaluated first. Environmental losses are computed with Equation 2.

$$Q_{env} = UA_{tank}(T_{env} - T_{tank})\Delta t \tag{2}$$

where UA_{tank} is the overall heat transfer coefficient between the water in the tank and the surrounding ambient air in $\mathrm{W/K}$, T_{env} is the environment temperature in C, T_{tank} the temperature of the storage media in C, and Δt is the simulation timestep in s. UA_{tank} can be computed by evaluating a simple series resistance network between the storage media and the environment, as shown in Equations 3–4. The tank base, lid, and wall insulation thermal resistances were all provided by the tank manufacturer. Appendix 5.1 tabulates the ice tank model parameter values.

$$UA_{tank} = \mathrm{R}_{tot,tank}^{-1} \tag{3}$$

$$R_{tot,tank} = \left(\mathrm{R}_{tot,lid}^{-1} + \mathrm{R}_{tot,base}^{-1} + \mathrm{R}_{tot,wall}^{-1}\right)^{-1} \tag{4}$$

The effects of free convection of water and air were also included in the computation of Equation 4, with convection coefficient values of 10 $\mathrm{W/m^2{-}K}$ and 100 $\mathrm{W/m^2{-}K}$ used for the inner and outer surfaces, respectively. Note that the effect of free convection is relatively small in comparison to the dominant conduction resistance of the tank insulation, and therefore fixed values are acceptable.

Energy transfer between the glycol and the water in the tank is computed by Equations 5 and 6.

$$Q_{glycol} = \varepsilon Q_{max} \tag{5}$$

$$Q_{max} = \dot{m}_b c_{p,f} \left(T_{b,in} - T_{tank}\right) \Delta t \tag{6}$$

where ε is the heat exchanger effectiveness, Q_{max} is the maximum possible energy transfer at any given timestep in J, $\dot{m}_b$ is the glycol mass flow rate in $\frac{\mathrm{kg}}{\mathrm{s}}$, $c_{p,f}$ is the glycol specific heat in $\frac{\mathrm{J}}{\mathrm{kgK}}$, and $T_{b,in}$ is the glycol inlet temperature in C. Heat exchanger effectiveness can be computed from Equations 7 and 8. Equation 8 is a standard effectiveness-NTU relation for a heat exchanger with one fluid having an infinite heat capacity [18].

UA_{hx} is a function of the SOC, S. (Eq. 9). The coefficients c_{mode} are different for discharging and charging modes, and were determined by minimizing the sum of the squared error of cumulative glycol heat transfer, in Wh, of the model and the respective charging and discharging experimental data shown in Section 2.1.2.

$$\varepsilon = 1 - \exp(-NTU) \tag{7}$$

$$NTU = \frac{UA_{hx}}{\dot{m}_b c_{p,f}} \tag{8}$$

$$UA_{hx} = c_{\text{mode},0} + c_{\text{mode},1}S + c_{\text{mode},2}S^2 + c_{\text{mode},3}S^3 \tag{9}$$

The tank heat storage media temperature (T_{tank}) and the SOC (S) are updated at each timestep by an energy accounting process. The total change in internal energy of the heat transfer media, $dU = M_f du$, in J, was compared against the energy required to fully accomplish each phase of tank charging or discharging, i.e., sensible liquid ($T_{tank} > 0$°C; $S = 0$); latent ($T_{tank} = 0$°C; $0 \leq S < 1$); and sensible solid ($T < 0$°C; $S = 1$). If the total internal energy change was less than the energy required to complete one phase, all the energy change is applied to that phase. T_{tank} is updated for the sensible phases and SOC updated for the latent phase. At the timestep when dU was greater than the remaining energy available for a given phase, the energy required to complete that phase is deducted and the remaining available internal energy change was applied to the next phase. The fixed value $h_{if} = 334\text{kJ/kg}$ was used for water's latent heat of fusion and $c_{p,ice} = 2030\text{J/kgK}$ for the specific heat of ice.

2.1.2 Ice Tank Model Calibration

The ice tank model was calibrated using charge and discharge experiments on a single 6265-L ice tank coupled to a glycol stream with an internal coil (CALMAC 1190; nominal capacity = 570 kWh). The ice tank was charged with a 30-ton variable speed chiller and discharged with facility hot water, which was controlled to mimic a building load. The ice tank was charged at a single rate because of chiller capacity limitations. A simplified schematic of the experimental facility is shown in Figure 2. The setup also included a variety of temperature, pressure, and flow rate sensors to measure the thermodynamic states leaving each component in the system.

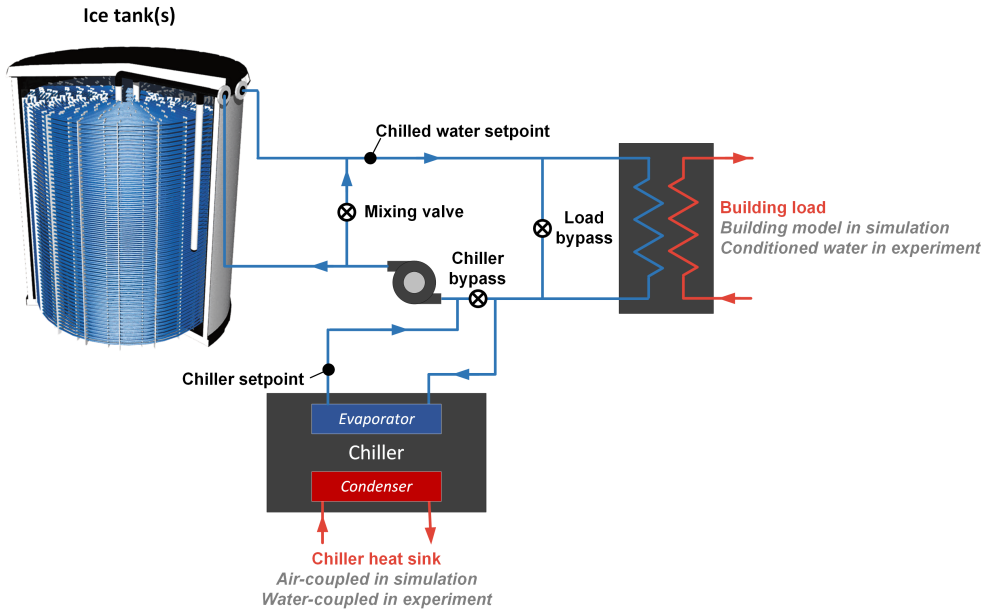

Figure 2: Chiller and ice tank plant schematic used in both the experimental and modeling efforts. Differences between how the building load was simulated and how the chiller was cooled are noted.

During charging the load bypass valve was open and the mixing valve was closed, forcing all the cold glycol from the chiller through the ice tank. The chiller compressor speed was controlled based on the glycol outlet temperature (chiller setpoint in Figure 2). The results from the charging experiment are shown in Figure 3 (left). Initially, the ice tank inlet temperature drops rapidly as the water in the tank sensibly cools. After two hours, the ice tank starts to freeze after briefly subcooling. For the remainder of the experiment, the glycol

temperatures slowly drift down as a thermal insulating ice layer forms around the tubes. After charging, the ice tank was discharged at a constant heat transfer rate. The chiller was off, the chiller bypass valve was opened, and the load bypass valve was closed. The heat transfer rate was maintained by controlling the mixing valve, thereby modulating the flow rate through the tank to account for changes in the outlet glycol temperature.

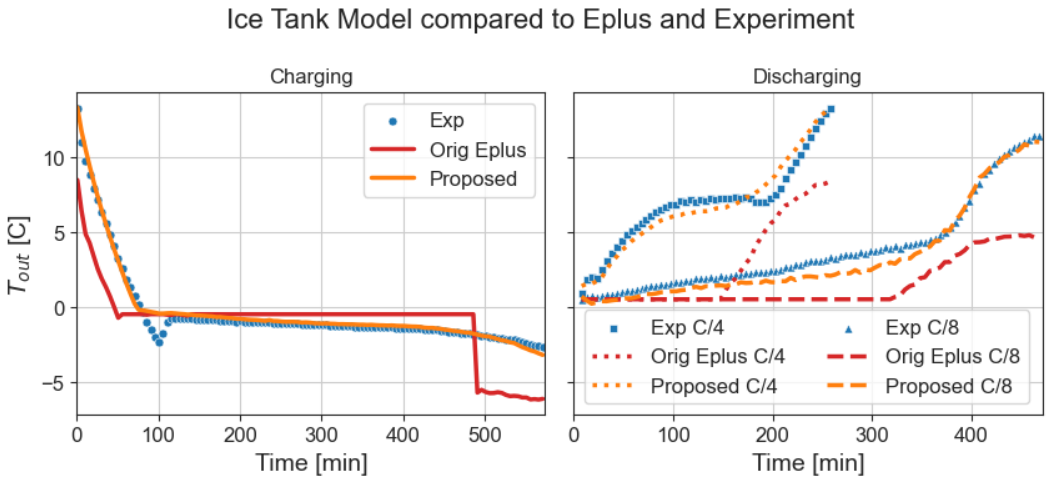

Figure 3: Ice tank outlet temperatures during charging (left) and discharging (right) at 4-hr (C/4) and 8-hr (C/8) rates

The proposed model was calibrated with the 4-, 6- and 8-hour discharge data, and the results are shown for the 4-hour (C/4) and 8-hour (C/8) data in Figure 3 (right). The existing ice storage tank model (red) is unable to track the measured data, whereas the proposed model has some error but tracks much more closely (orange). The root mean square errors of the existing model were 2.12, 4.62 and 2.9 °C for charging, C/4 discharging and C/8 discharging; the max errors were 5.3, 6.7 and 6.8 °C, respectively. For the proposed model, the RMSE were 0.38, 0.72, and 0.69 °C and the max errors were 1.9, 1.4, and 1.4 °C, respectively. Appendix 5.2 contains detailed plots of the validation.

Since the experiment tested a limited set of conditions, the validity of the model for designs outside the experiment cannot be ascertained. Instead of extrapolating the parameters for tanks with far different sizes, multiple tanks are used in parallel to handle the simulation of a larger capacity tank. The chilled water loop flow is split among the tanks equally and the operation of each tank is identical, therefore simulating only a single tank is sufficient.

In Appendix 5.6, the operation of the ice tank model by the MPC and schedule control strategies is verified to be within bounds of the experimental C-rates.

2.2 Building Models

The ice tank model described above is run within building models using the whole-building energy simulation program, EnergyPlus, which predicts energy consumption accounting for the interactions between climate, internal gains, building form and fabric, HVAC systems, and renewable energy systems [19].

The building model used is based on a U.S. Department of Energy (DOE) Commercial Building Prototype model for the Medium Office, which represents a typical building rather than a specific building [20]. As published, the model does not contain the chilled water-based cooling system needed for coupling with an ice tank, so the cooling system from the Large Hotel Prototype was substituted for the direct expansion cooling

system in the published Medium Office Prototype. The chilled water-based cooling system is composed of an air-cooled chiller, a circulating pump, and a water-to-air heat exchanger inside each of the three air handlers. The EnergyPlus chiller model used here is the "electric EIR chiller," an empirical model that uses performance curves along with information at rated conditions to determine performance at off-rated conditions [21]. The size of the chiller required a two-tank system with a total capacity of 1140 $\mathrm{kWh_{th}}$ because the flow rate of the chilled water loop is 8.7 kg/s, whereas that of tank is 4.5 kg/s. EnergyPlus's PVWatts object, based on SAM's PVWatts [22], was used to simulate the energy production of a 150 kW ground-mounted PV array with typical poly- or mono-crystalline silicon modules.

This paper will refer to three building models: (1) the *base building model* consists of the modified medium office building; (2) the *schedule-control building model* is the modified medium office building with two ice tanks, and where the chiller setpoints are set by the schedule control; and (3) the *MPC building model*, for which the setpoints of the chiller and the chilled water are set following the Optimal case. Building models 2 and 3 follow the schematic shown in Figure 2, except there are two tanks.

2.3 Utility Rate Cost Calculations

We used typical meteorological year three (TMY3) EnergyPlus weather files from three U.S. cities in climate zone 3B—San Diego, CA; Las Vegas, NV and El Paso, TX. Their utility rates were selected for having different emphasis of the TOU energy, TOU demand, and monthly demand components.

TOU energy is calculated using a net billing method in which energy is purchased at a buy rate and any exported energy is sold at a sell rate. In our case the buy rate and sell rates are always equal to each other, but they vary by TOU period. Thus, the monthly TOU energy charge is the sum of net energy purchased/sold [kWh] multiplied by the energy rate [$/kWh] for each period. TOU demand is calculated as the sum of the peak demand [kW] per period times the demand rate [$/kW] for that period. Finally, monthly demand is the peak demand [kW] of the month times the monthly demand rate [$/kW].

- San Diego's "San Diego Gas and Electric AL TOU2 Secondary": All three components (TOU energy, TOU demand, and monthly demand) are expensive and the TOU variation is high. [23]
- Las Vegas's "Nevada Power Company ME OLGS 1 TOU": Low TOU and monthly demand rates and medium TOU energy rates. [24]
- El Paso's "El Paso Electric Company General Service Rate – TOU Secondary Voltage": Medium monthly demand rates, no TOU demand, and low but variable TOU energy rates. [25]

The typical spring, summer, and autumn weeks from the weather file were simulated using the rate structure for that given time period. TES simulations were not performed for a winter week as the TES would not be operating. Instead of a full year, the typical three weeks were simulated and then extended to a year to allow a focus on the weekly results and the relationship of the three seasons to the annual. When extending from representative weeks to a year, it is unclear which weeks belong to which season—and even if all weeks could be categorized by season, the rate structure does not necessarily follow the same categorization. To avoid the complexity of categorizing each week by both climate and rate, uniform weighting was used to average the representative weekly utility cost into an annual cost with the following method. First, each season's weekly net load profile is repeated to make annual profiles, the costs of which are calculated using the System Advisor Model [22]. Then, for each of the four seasons, the month containing that season's representative week is selected as that season's representative month (e.g., August for summer). Finally, the costs of each season's representative month are multiplied by three and summed for the annual cost. Figure 4 shows location characteristics for a day in the representative summer week.

To estimate the error using this approach, annual simulations were run for the base, schedule, and optimal cases (the MPC case was not run). As this study is focused on savings relative to the base scenario, the

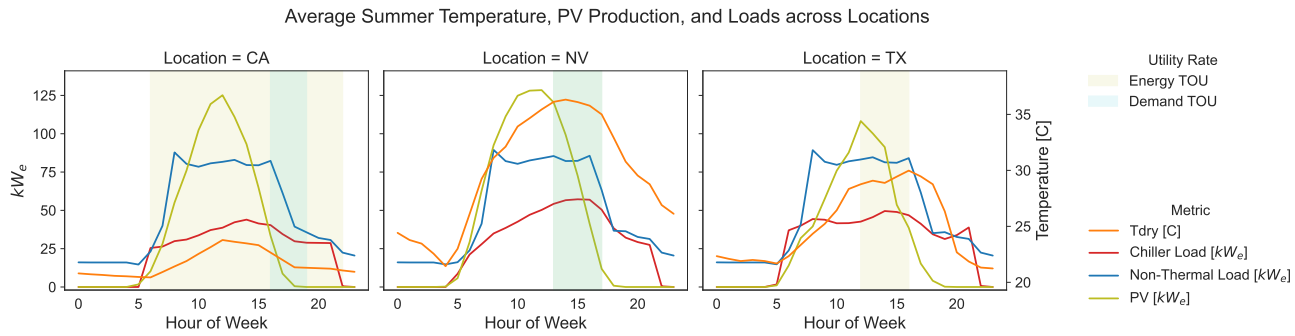

Figure 4: Location characteristics and the energy and demand time-of-use peak period for a day in representative summer week. Non-thermal load does not depend on location.

difference in savings between the two calculation methods is more relevant. The difference in chiller plant operating costs averaged 15% with a range of 2-47% whereas those of the savings averaged 6% with a range of 0-15%, which is reasonable for the purpose of analyzing control strategies over example scenarios.

The cost of operating the chiller plant is distinguished from the cost of operating the entire building. In order to isolate the cost of operating the chiller plant, a non-thermal load is created by removing the chiller plant load from the building load to establish a hypothetical minimum cost of operating the building. While the demand costs of this hypothetical minimum are reachable by shifting the chiller plant load to prevent peak overlaps with the non-thermal load, the energy costs are not an achievable minimum. Although the thermal load can be shifted to cheaper times, it cannot be avoided and more so, usually increases slightly because the low charging temperature makes charging less efficient than using the chiller to meet the load directly.

2.4 Controls

Here we discuss the two types of controls—schedule-based control, which is a typical clock-based schedule strategy, and non-linear MPC, which we applied in this study. This paper presents an optimization model of the TES, chiller, and building. The mathematical formulation of the utility rate cost is described in [26]. The schedule is adapted for each location depending on the building load and the utility rate, but is the same regardless of the presence of PV.

2.4.1 Schedule-Based Controls

The schedule-based controls use only the utility rate schedule and building occupancy schedule and are pre-set prior to the simulation. The procedure is based on peak-day analysis when sizing an ice storage system: done upfront, and once determined, fixed for each simulation. The schedule control specifies the duration and setpoints for the three possible modes: idle, charge, and discharge. During the occupied hours of 8 AM to 8 PM, the cooling plant provides 6.7°C water to the building. This chilled water setpoint is met during idle mode by just the chiller, and in discharge mode can be met by just the ice tank, or the chiller and ice tank.

Operation of the chiller depending on control model is as follows. During the idle mode, the TES is not being charged or discharged, but the chiller will turn on to meet the setpoint when the return temperature from the building (T_{ret}) requires cooling (i.e., identical to the baseline). During charge mode, the chiller setpoint is fixed at -3.8°C. The tank charges during the nighttime off-peak, unoccupied hours. Charging is tapered down by increasing the chiller setpoint to 6.7°C, and the ice tank enters idle mode. The chiller setpoint temperature during discharge mode is set to >6.7°C to trim the chiller load to ensure the ice tank provides

the rest of the cooling to achieve the 6.7°C setpoint. The TES valve is controlled to ensure this setpoint is met.

The chiller discharge setpoint is determined by a one-time parametric sizing simulation using the peak day load and the utility rate peak pricing window. Peak day simulations are executed with a systematic incrementing of the chiller setpoint until the ice tanks reached zero SOC at the end of the peak pricing window. This chiller "setup" setpoint temperature is unique for each climate zone and utility rate.

For utility rates with a peak period, the tank discharges during the afternoon peak window. For flat utility rates, the tank discharges to reduce the load during the occupied hours. For El Paso, the rate is always flat. For Las Vegas, the rate has a peak window in the summer months (June-September) and is flat otherwise. For San Diego, there is a year-round peak window.

The schedule-based controls for Nevada are illustrated in Figure 5. In spring and autumn, there is no peak period and the tank discharges between 7:30 AM and 8:30 PM. The autumn load is slightly lower, so the charging period finishes earlier than in the spring. In the summer, the tank only discharges during the peak period, is idle during the morning hours, and requires a longer charge window. Plots showing the schedule for San Diego and El Paso are found in Appendix 5.4.

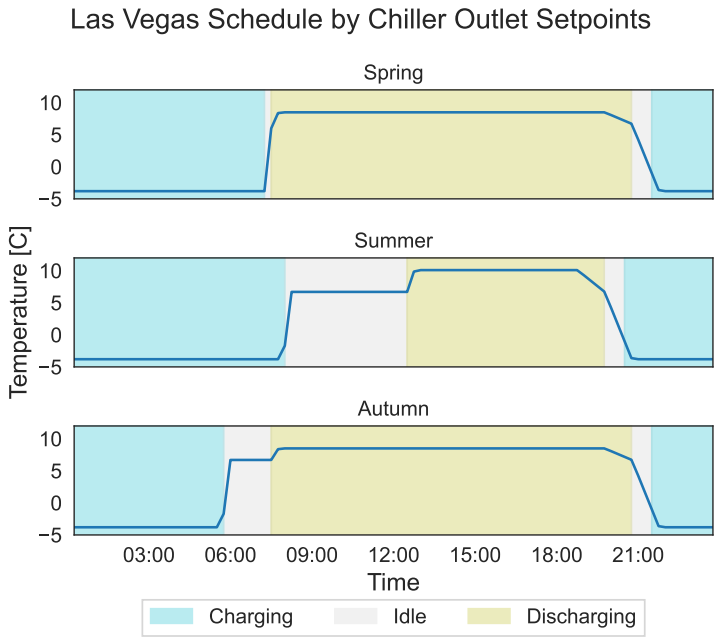

Figure 5: Schedule-based controls for Las Vegas, Nevada

2.4.2 Non-Linear Model Predictive Control

The MPC is formulated as a relaxed mixed-integer non-linear program (MINLP) that represents nearly exactly the ice tank model and its different modes of charging vs. discharging and latent vs. sensible cooling. The optimization problem represents the chiller power as a polynomial regression dependent on the temperature drop across the chiller and the temperature of the condenser inlet. The prediction and control horizons are both 24 hours at 15-min intervals and roll through 7 days. The time-dependent forecasts taken from the base simulation include the temperature of the condenser inlet; the temperature increase of the chilled water due to the building cooling load, which serves as a proxy for the cooling load given that the flow rate

is constant; the non-thermal load; and the PV generation. The model inputs include ice tank and chiller parameters, utility rate costs and regularization parameters, explained in the next paragraph. The control variables includes temperatures at the inlet and outlet of the tank, chiller and chilled water branch; tank SOC, mass flow rate, and charge or discharge rate; and chiller power.

Regularization was added to produce smoother, more realistic operation without oscillations and steep changes in the chilled water temperatures and the chiller operation. This was done by constraining the variation of three quantities: the first and second derivatives of the tank inlet temperature and the chilled water setpoint temperature with respect to time; and the max difference in the temperature drop across the chiller between timesteps. These regularized solutions have slightly worse optimal points by a few percentage points but the smoother operation is easier for a chiller to follow (including the EnergyPlus modeled chiller) and thereby result in MPC building model performance closer to that predicted by the optimal case.

The MINLP was relaxed to an NLP to reduce solve time. Solving the full MINLP with the BONMIN (Basic Open-source Nonlinear Mixed Integer programming) solver [27] often exceeded an hour, whereas the NLP with binary penalties solved in a few seconds with the Interior Point Optimizer (IPOPT) solver [28]. Binary penalties were added to the objective to push the relaxed binary variables toward 0 or 1. In several timesteps, the values will be between 0 or 1. While these relaxed solutions are not in the feasible space of the MINLP, they proved to be near enough such that once these solutions (the optimal case) are passed into the MPC building model, the simulation is able to follow the setpoints with only small deviations.

The objective is to minimize the sum of three terms: utility costs, regularizations, and binary penalty. The cost of the binary penalty and the costs of the regularizations are hyperparameters that tune their relative importance to the cost of the utility bill. The full set of system parameters, variables, and equations is presented in Appendix 5.5 and is implemented using the optimization modeling package Pyomo [29].

An initialization scheme provides the solver with a feasible starting point by using the SOC profile of the schedule simulations. While the resulting starting point does not follow the schedule exactly and may have some points of infeasibility across timesteps, the solver is able to converge for the full problem. From experiments with different SOC profiles, it often converges to a very similar solution regardless of the starting profile, provided it is close to the feasible region.

2.5 Tank Simulations with Optimized Setpoints

The ice tank was integrated with EnergyPlus via a user-defined plant component object and the control strategies' operating setpoints are actuated via the Python Plugin system, a feature that provides a way to develop custom control and modeling routines. A user-defined component is a shell for creating custom HVAC equipment models that simulate alongside other EnergyPlus plant components, thereby providing a method of modeling types of equipment that do not have built-in EnergyPlus models [30]. The ice tank model attempts to operate such that the plant outlet temperature meets the control setpoint temperature by adjusting the mixing value fraction. It then updates its tank temperature and SOC, and provides the outlet temperature of the user-defined component object to EnergyPlus. At the end of the week-long simulation, the chiller electricity use, tank SOCs, and chilled-water loop temperatures are reported by EnergyPlus.

2.6 Sensitivity Analysis

For a sensitivity analysis of cost and savings to climate and rate, hypothetical mixed-location scenarios were created by mixing the CA climate with NV rate, and NV climate with CA rate. Each is run with both PV and no PV and with schedule controls and MPC for 16 scenarios. The schedule was adapted for the new rate following the same parametric method in Section 2.4.1. The MPC results use the predictions from the

optimization problem ("Opt") instead of the MPC building simulation ("MPC") to avoid prediction errors in the analysis. These mixed-location scenarios are compared with the single-location scenarios to determine the impact of NV being warmer than CA and CA being costlier than NV.

3 Results

Section 3.1 shows the load shift profiles and the impact on chiller plant operating costs by the controls for summer in San Diego. Section 3.2 examines savings across the three locations and between PV and TES. Section 3.4 contains sensitivity analysis of cost and savings to climate and utility rate.

3.1 Representative Summer Month in San Diego, CA: MPC Lowers Electric Bill

This section shows how the operation is adjusted by the controls. The timeseries results are based on the week-long simulation, but the chiller plant operating costs are for the representative summer month, following the methodology in Section 2.3.

3.1.1 Energy, Load, and SOC

In Figure 6, we compare the four cases: (1) the optimal solution from the solver described in Section 2.4.2 ("Opt"), (2) the simulation of the MPC building model ("MPC"), (3) the simulation of the schedule-control building model ("Schedule") and (4) the base building model without TES ("Base"). The building models are described in Section 2.2.

Only a single weekday of the summer representative week is plotted for clarity; Appendix 5.7 contains the week-long plots. The left column shows the No PV case, the right the PV case. Each columns' figures are split into three subplots. The first shows the Total Load, composed of the chiller load that is modified by each control strategy, non-thermal load and PV generation when applicable. The second shows only the chiller load, and the third shows the ice tank SOC. The lightly shaded gray area is the shoulder peak period where the TOU energy charges are slightly higher (11.4¢/kWh vs 9.0¢/kWh), whereas the darker shaded gray area is the on-peak period with highest charges for both TOU energy (16.9¢/kWh vs. 11.4¢/kWh) and TOU demand ($26.8/kW vs. $0/kW). The monthly demand is $52.8/kW.

For the No PV scenario, the flattening of the daytime building load by the MPC compared to the base and schedule in the first subplot shows that the MPC is especially focused on monthly demand because it is about twice as expensive as the TOU demand. Shown in the second subplot, the MPC reduces TOU demand by focusing on the highest 15-min periods at the beginning of the peak period, rather than reducing the chiller load during the entire peak period to zero as the schedule does. The third subplot shows that the MPC uses the entire SOC range of the tank, has far less idle time, and charges at a faster rate. The entire tank is required during this summer week so dynamically allocating SOC to the most valuable times is critical for balancing trade-offs among savings in the three cost components. In contrast, the schedule does not use the entire tank as it was designed to discharge during the short peak period and does not reduce the monthly demand.

In the PV scenario, right side of Figure 6, the load is significantly reshaped by PV such that it can be easier to reduce monthly demand. The residual load has a tall and narrow peak in the early morning and in the evening, the latter of which coincides with the peak period. Because the schedule turns off the chiller at this time, it concurrently minimizes TOU and monthly demand. However, the scheduled charging in the

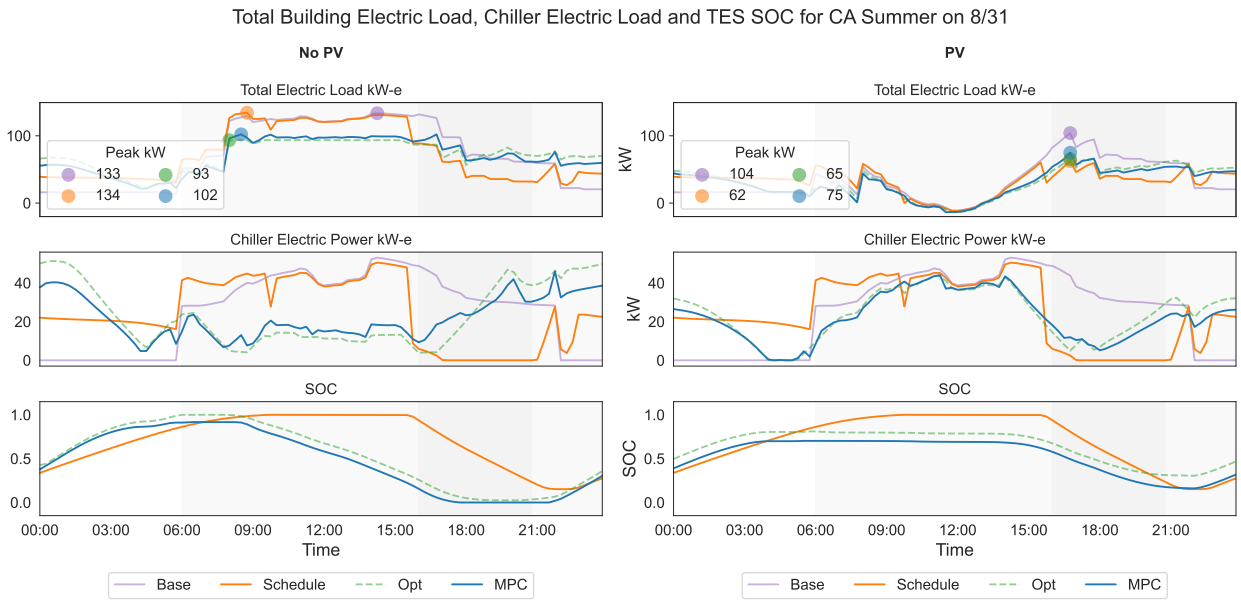

Figure 6: First day of the summer representative week for San Diego, CA No PV. TOU periods shown by grey

morning hours can sometimes overlap with the morning load, preventing the schedule from reducing the monthly demand as far as the MPC does. The SOC subplot shows a smaller SOC range for the MPC.

Figure 6 also shows the ability of the optimization model to predict ("Opt") and control the simulated loads within the MPC building model ("MPC"). In the first and second subplots, the chiller prediction overestimates the power at high loading factors and underestimates the power at low factors. The chiller model in EnergyPlus has controls around low loading factors, ramping, and cycling that are not represented in the MPC regression model, leading to unpredictable behavior when dynamically reducing the chiller load to near zero. Thus, it is impossible to flatten the load to the Opt values and the monthly and TOU demand are higher. In the third subplot, the ice tank model follows the control setpoints with small deviations from the predicted SOC, showing that the tank's dynamics are adequately represented by the optimization model. Prediction errors in the ice tank state and the building thermal load may compound when the chilled water loop operates at temperatures different from forecasted. Even so, the deviations are small and the MPC adequately predicts and controls the TES system in the EnergyPlus simulation for load management. Using a shorter control window to reset and align the optimization with the simulation will reduce the accumulation of error over time.

3.2 Electric Bill Savings Breakdown for the Three Locations

In this section, we examine the chiller plant operating costs. The results here are per season month and per year using the calculation method described in Section 2.3.

3.2.1 Savings for Three Seasons in San Diego, CA

Figure 7 shows the monthly savings per charge type for the Base, Schedule, MPC, and Opt cases for each season, with No PV (left) and with PV (right). The percent change annotated inside the bar for each compo-

nent is relative to the component cost of the base case. The total savings annotated outside to the right of the bar is relative to the total cost of the base case. Appendix 5.8 contains similar plots for El Paso, TX and Las Vegas, NV.

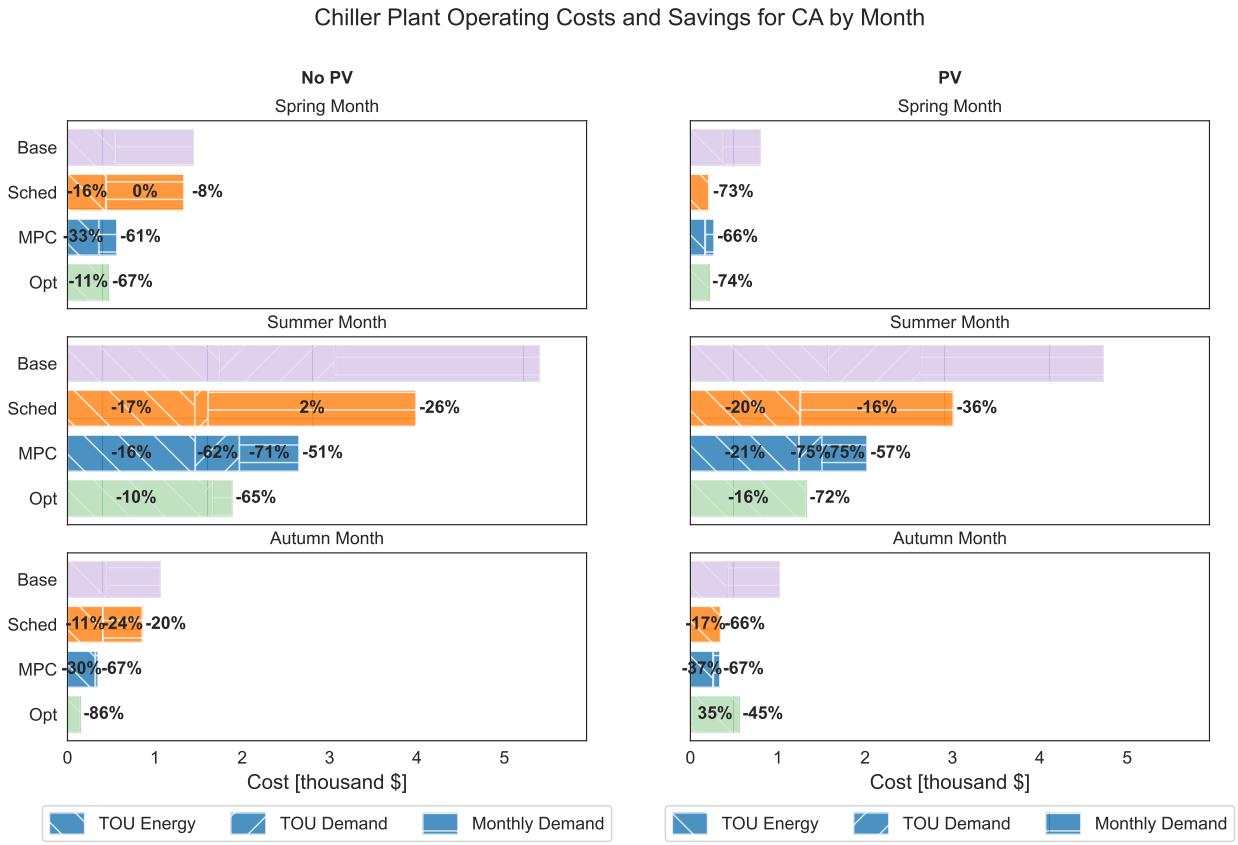

Figure 7: Chiller plant operating costs in thousand dollars (bar width) and savings percent (annotated) for San Diego

For No PV, the greatest savings are in the monthly demand, achieved to a larger degree by the MPC than the schedule. Energy cost savings are more moderate but the MPC still achieves larger savings. For TOU demand, the savings are smaller and the schedule performs better. The schedule is not designed for flattening the monthly demand and misses out on significant potential savings; in fact, the resulting peak is very slightly higher (134 kW for the schedule vs. 133 kW for the base case) due to the shoulder period when the tapering charging overlaps with a high load period in the early morning. The minimum demands are not achievable by the optimization because the tank is not large enough, but are achieved in the PV scenario below.

For the PV scenario, the optimal case is able to reach the minimum TOU and monthly demand because the total energy requirement of the load is within the capacity of the ice tank. The schedule achieves the minimum TOU demand, and performs better at reducing monthly demand than in the No PV scenario. In the MPC case, the prediction error during the evening peak when the simulated chiller does not turn down as low as predicted by the optimization reduces demand savings.

Particularly for flattening the load, any deviation from a constant load will result in error, making demand extremely sensitive to these errors. The MPC total costs differ from the optimal total costs by at most 19% with a 13% average for the No PV scenario. For PV, the prediction error is at most 22% with a 13% average. Since the schedule sets the chiller setpoints directly in EnergyPlus and the chiller is turned off completely during the TOU window, the schedule is able to reduce the TOU demand better than the MPC.

Comparing savings across the No PV scenarios, the MPC gives an average total savings of 60% whereas the schedule gives 18%. With PV, the MPC gives an average total savings of 63% whereas the schedule gives 58%. The savings potential of spring and autumn are much less than for summer. The optimal savings in spring and autumn are between 14% and 28% with an average of 21% of the optimal savings in summer. The schedule savings in spring and summer are between 8% and 39% with an average of 34% of the schedule savings for summer. The MPC savings are between 20% and 32% with an average of 26%. During these seasons, the thermal loads are smaller while the utility rate charges are cheaper and may not have an on-peak period. The control setpoints need to be modified to account for these changes, and the simulations show depths of discharge much less than 90%. That in addition to reduced savings during the off seasons results in less potential value for the same size TES, a consideration that will impact the economic benefit.

3.2.2 Annual Savings Breakdown Across the Three Locations

Table 1: Savings percent relative to the base case of the annual chiller plant operating cost for the MPC and schedule, and their unnormalized difference

	San Diego		Las Vegas		El Paso	
Savings [%]	No PV	PV	No PV	PV	No PV	PV
Sched E_{TOU}	-15	-23	-27	-27	-25	-27
Sched D_{TOU}	-89	-100	-76	-79	-	-
Sched D_{Mnt}	-3	-43	-45	-52	-56	-37
Sched Total	-22	-45	-35	-34	-46	-33
MPC E_{TOU}	-22	-29	-30	-25	-38	-33
MPC D_{TOU}	-63	-75	-80	-82	-	-
MPC D_{Mnt}	-76	-77	-66	-77	-76	-83
MPC Total	-55	-60	-39	-35	-63	-66
Diff E_{TOU}	-6	-6	-3	2	-13	-7
Diff D_{TOU}	26	24	-4	-2	-	-
Diff D_{Mnt}	-73	-34	-21	-25	-20	-46
Diff Total	-33	-14	-5	-1	-17	-32

The annual savings per cost component for each scenario is shown in Table 1. The differences are calculated as savings percent of MPC less that of the schedule. For all scenarios, the MPC has higher monthly demand savings than the schedule. For TOU demand, the schedule has significantly greater savings in CA. For TOU energy, the MPC performs moderately better than the schedule.

The smallest overall savings are found in Las Vegas, which is dominated by energy costs. The savings in the TOU energy for the MPC and the schedule are similar. While the MPC is able to additionally reduce the monthly demand, the relative impact of those savings is small. The largest overall savings are found in El Paso, where the MPC outperforms in both components especially monthly demand. San Diego offers large savings as well, and the additional savings due to the MPC are as large as for El Paso. However, the San Diego No PV scenario is the only case in which the schedule was unable to produce appreciable monthly demand savings, thereby making the MPC's additional savings unusually high.

The percent savings due to TES with MPC are similar whether or not there is the 150-kW PV system, suggesting that the TES potential for savings is separate from that of PV. PV reduces primarily the energy cost while reshaping the load so that the residual peak occurs during the TOU window, which limits the ability of the PV to reduce TOU (and monthly when coincident) demand when the load continues after PV generation ends. Compared to PV, TES reduces demand to a higher extent than energy. Since PV and TES address different components of the utility bill, their individual effects on savings are more complementary than competitive

regardless of control type.

3.3 Scenario Comparison and Discussion

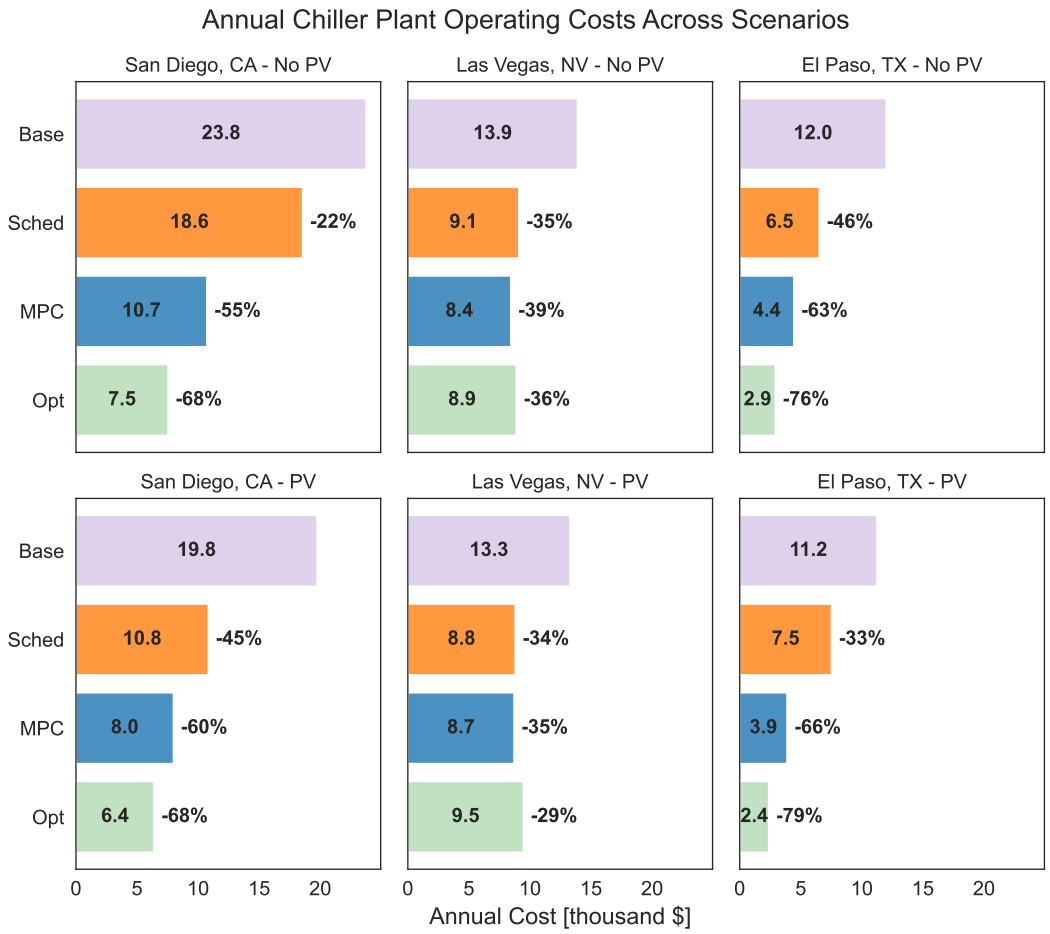

Figure 8: Annual chiller plant operating costs and savings for all locations with and without PV. Savings are relative to the base case.

When considering payback and return on investment, it is necessary to consider the magnitude of cost and savings, which are much larger in San Diego than in El Paso or Las Vegas. The annual chiller plant operating costs and savings are plotted in Figure 8. Overall, this 1140 $\mathrm{kWh_{th}}$ TES with MPC saves 35-66% on chiller plant operating costs relative to the base case, which can be as high as $13,010 for San Diego No PV or as small as $4,526 for Las Vegas with PV. The benefit of the MPC relative to the schedule can be 1-33%, which is worth as much as $7,859 for San Diego No PV or as little as $112 for Las Vegas PV. Whether or not it is an economic investment depends on the cost of purchasing and installing the TES and other financial parameters. Using the MPC control will likely reduce the optimal size of the TES by increasing the utilization and economic value of any given size.

It is also important to consider the savings to the chiller operating cost as a part of the total building utility bill cost. Appendix 5.9 contains the annual total building electric bill costs and savings. The TES with MPC saves 8-15% on the annual total cost with an average of 11.7% for No PV and 10.7% for PV. For the schedule, the average savings are ∼8% for both No PV and PV.

The control performances differ between the MPC and the schedule because the MPC, with load forecasting and mathematical optimization, can calculate the optimal tradeoff between utility rate components. A large monthly demand rate will incentivize flattening the total load over all periods whereas a large TOU demand/energy rate will incentivize shifting the total load out of the most expensive periods into the cheapest periods. The schedule, except in clear cases where the TOU component is dominant, cannot locate the balance point between these two types of demand charges. Performing tradeoffs in reducing different bill components is also more important when the tank is not large enough to fully offset the summer chiller load as was the case for the San Diego No PV scenario. The cost-benefit analysis of MPC includes the balance of the additional savings against the increased cost and complexity of deployment. The optimization for the MPC introduces forecast errors, sub-optimal solutions, and prediction errors that will reduce MPC savings relative to the Opt case.

Our results show that the MPC can be tuned so that the forecast errors are within a reasonable range to provide significant savings compared to a simple schedule. Forecast errors are not discussed here because the forecasts were nearly perfect. There is no way to guarantee reaching the global minimum for a nonlinear relaxation of a MINLP using regularization and penalties, but the Opt case often achieves the no-thermal load monthly and TOU demand when the ice tank is large enough. Between El Paso and San Diego, the Opt case is 68-79% of the way to the no-thermal load cost. The MPC prediction error, calculated as the difference between "MPC" and "Opt," was found to be reasonable with a 9% average, which shows that the most important parts of the system were well represented.

3.4 Sensitivity of Savings to Climate and Rate

While both a warmer climate and a more expensive utility rate lead to larger annual chiller plant operating costs, we analyze the sensitivity of the savings to each. Figure 9 shows the change of savings from the single-location scenario (rate and weather are the same) by changing the climate or the rate to the mixed-location scenario (rate and weather are mixed). In the "To Climate" column on the left, mixed-location scenarios where the climate is changed is plotted against the single-location scenario; the rate is not changed. These are categorized depending on whether the mixed-location climate is warmer (NV) or cooler (CA). Likewise in the "To Rate" column on the right, mixed-location scenarios where the rate is changed is plotted against the single-location scenario.

For instance, in the "To Climate" column, the CA-location, NV-rate scenario is plotted against the NV-location, NV-rate scenario under the "Cooler" color (California is cooler than Nevada). Conversely, the NV-location, CA-rate scenario is plotted against the CA-location, CA-rate scenario under the "Warmer" color (Nevada is warmer than California). In the "To Rate" column, the CA-location, NV-rate scenario is plotted against the CA-location, CA-rate scenario under the "Cheaper" color—these are using the same climate, but Nevada has a cheaper utility rate than California.

These plots are interpreted as follows. If the point falls on the 45° line, then the change from one climate to the other, or from one rate to the other, has no impact on the savings. If the point falls above the 45° line, then the change (e.g., to a costlier utility rate) increases the savings of the TES and the specified control strategy. If the point falls below the 45° line, then the change (e.g., to a cooler climate) decreases the savings of the TES and the specified control strategy. The distance from the 45° line indicates the magnitude of the change in savings.

The impact on savings by climate is stronger for the Schedule cases, which shows an average 15% change versus 7% for the Optimal cases. For the Schedule cases, the total savings (circles) change 7-22%. For the Optimal cases, the savings change 2-19%. Rate has a bigger impact than climate and more so for the Optimal cases. For Optimal, the savings change 45-60% while for Schedule, the savings change 22-41%.

The contribution of the three cost components (small triangles) highlights the complexity of comparing

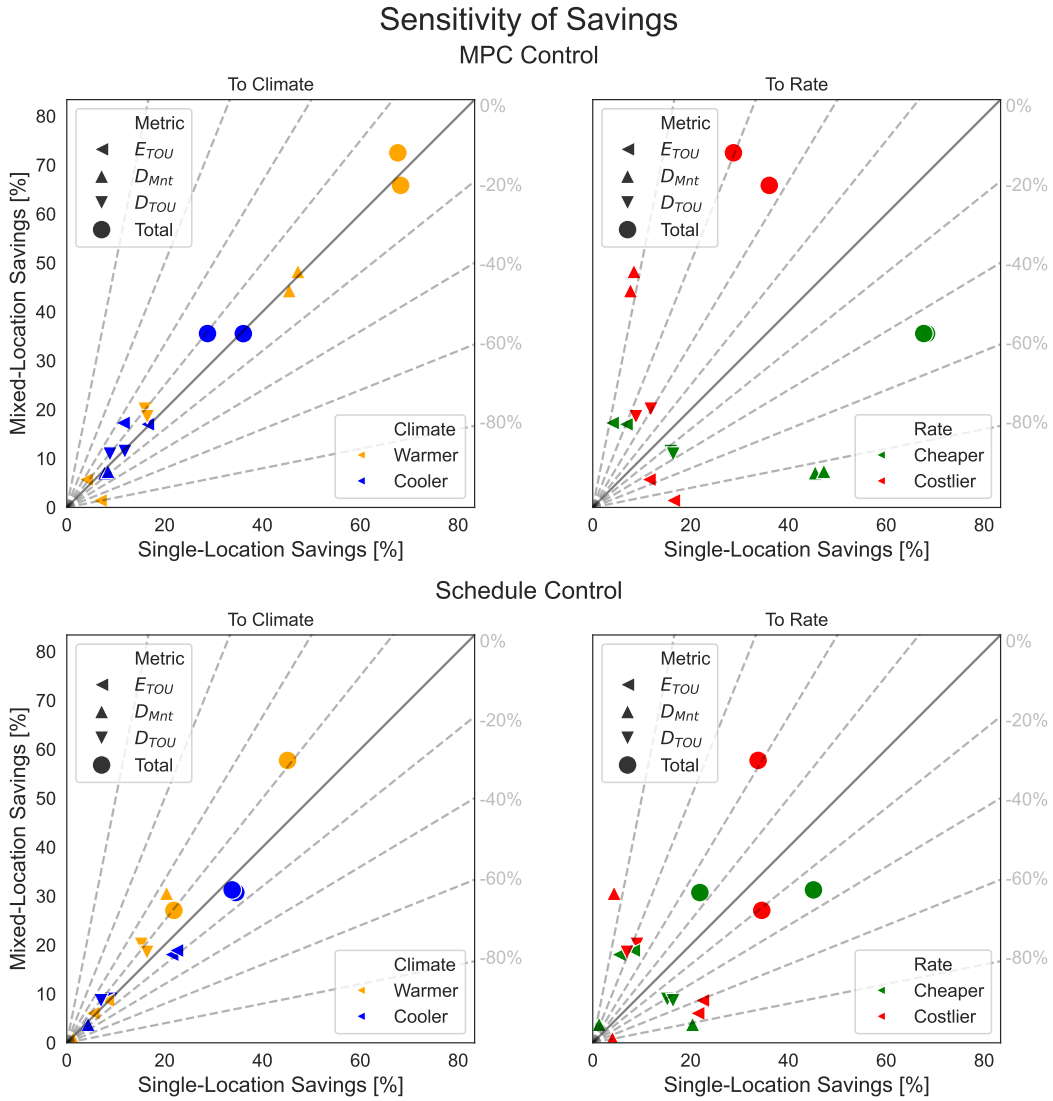

Figure 9: Sensitivity of annual normalized savings (percent change of percent savings) by utility cost component. The values of each component cost (smaller triangles) sum to the total (larger circle).

across different rates. For the Optimal cases, switching to the cheaper, energy-dominant NV rate (green), means TOU energy savings improve but demand savings are reduced; on balance, the total savings are smaller. The opposite is true for switching to the more expensive, demand-dominant CA rate. For the Schedule cases, the trends of the changes in the component costs have a very similar direction, but on balance the total savings could be higher or lower.

Overall, the Optimal case savings are much more sensitive to rate than to climate, while the Schedule case savings are slightly more sensitive to climate than rate. The strengths of the control strategy will determine whether climate or rate is more important for its performance. These results show that the interplay of control strategy and complex TOU rates makes it difficult to predict the impact on savings intuitively.

4 Conclusion

This study examined the impact of MPC versus schedule control on the cost of operating a chiller plant with ice TES for scenarios with complex utility rates and on-site PV. Our results show that MPC can get close to the no-thermal load minimum costs, outperforming the schedule-based control and saving 35-66% on the chiller plant operating cost.

In demand-dominant rates like San Diego and El Paso, MPC can reduce the cost by 68-79%, but in the energy-dominant Las Vegas rate, the cost was only reduced by 29-36%. Compared to the schedule, MPC was found to offer additional savings of 1-33% with an average of 17%. The schedule performs well in energy-dominant rates, matching the MPC savings. The schedule outperforms the MPC in TOU demand reduction in one scenario but had far smaller savings in monthly demand overall.

While the economic benefit of the ice tank is highly dependent on the controls, it is not dependent on the presence of PV. The large savings during the summer months are moderated by the remainder of the year where thermal loads and rate charges are less extreme. For both controls, the spring and autumn savings were only 22% on average of those in the summer.

The optimization model can achieve both the minimum TOU and minimum monthly demand costs by demand management while reducing TOU energy costs by energy arbitrage. The optimization produces control sequences that are realistic enough that the MPC building model can follow them with prediction errors averaging 9%. Errors in the chiller prediction lead to the simulated chiller load being higher than predicted, with commensurate reductions in demand savings. These errors are due to chiller behaviors around low load, ramping and cycling that were not represented in the model but which are important for accurately predicting how to dynamically minimize chiller load. By contrast, the schedule control as implemented in this study is not subject to such errors but lacks foresight into the overall load. Field studies to understand how the MPC would perform under real operating conditions are recommended.

Acknowledgments

This work was authored in part by the National Renewable Energy Laboratory, operated by Alliance for Sustainable Energy, LLC, for the U.S. Department of Energy (DOE) under contract no. DE-AC36-08GO28308. The views and opinions of the authors expressed herein do not necessarily state or reflect those of the U.S. government or any agency thereof. Neither the U.S. government nor any agency thereof, nor any of their employees, makes any warranty, expressed or implied, or assumes any legal liability or responsibility for the accuracy, completeness, or usefulness of any information, apparatus, product, or process disclosed, or represents that its use would not infringe privately owned rights. Funding provided by the Buildings Technologies Office and the Assistant Secretary for Energy Efficiency and Renewable Energy.

5 Appendix

The appendix is organized as follows. Section 5.1 shows the parameters of the ice tank model. Section 5.2 shows validation of the effectiveness-NTU ice tank model. Section 5.3 has details on the three utility rates. Section 5.4 shows the schedule controls for San Diego and El Paso. Section 5.5 describes the optimization model mathematical formulation. Section 5.7 contains timeseries for summer weeks of the three locations. 5.8 shows the savings breakdown for Las Vegas, NV and El Paso, TX. 5.9 compares the total building cost among scenarios.

5.1 Ice Tank Model Parameter Values

Table 2: Tank model parameter values

	Parameter	Definition	Unit
D	Tank diameter	2.261	m
H	Tank height	2.565	m
V	Fluid volume	6.264	m^3
R_{lid}	Lid area-specific resistance	4.227	$\frac{\mathrm{Km}^2}{\mathrm{W}}$
R_{base}	Base area-specific resistance	1.585	$\frac{\mathrm{Km}^2}{\mathrm{W}}$
R_{wall}	Wall area-specific resistance	1.585	$\frac{\mathrm{Km}^2}{\mathrm{W}}$
$A_{s,lid}$	Lid surface area	$\frac{\pi}{4}D^2$	m^2
$A_{s,base}$	Base surface area	$\frac{\pi}{4}D^2$	m^2
$A_{s,wall}$	Wall surface area	πDH	m^2
$R_{tot,lid}$	Lid total resistance	$\frac{R_{lid}}{A_{s,lid}}$	$\frac{\mathrm{K}}{\mathrm{W}}$
$R_{tot,base}$	Base total resistance	$R_{tot,base}$	$\frac{\mathrm{K}}{\mathrm{W}}$
$R_{tot,wall}$	Wall total resistance	$\frac{R_{wall}}{A_{s,wall}}$	$\frac{\mathrm{K}}{\mathrm{W}}$
$c_{\text{chrg},0}$	Charging UA coefficient 0	4.950×10^4	$\frac{\mathrm{W}}{\mathrm{K}}$
$c_{\text{chrg},1}$	Charging UA coefficient 1	-1.262×10^5	$\frac{\mathrm{W}}{\mathrm{K}}$
$c_{\text{chrg},2}$	Charging UA coefficient 2	2.243×10^5	$\frac{\mathrm{W}}{\mathrm{K}}$
$c_{\text{chrg},3}$	Charging UA coefficient 3	-1.455×10^5	$\frac{\mathrm{W}}{\mathrm{K}}$
$c_{\text{dchrg},0}$	Discharging UA coefficient 0	1.848×10^3	$\frac{\mathrm{W}}{\mathrm{K}}$
$c_{\text{dchrg},1}$	Discharging UA coefficient 1	7.429×10^4	$\frac{\mathrm{W}}{\mathrm{K}}$
$c_{\text{dchrg},2}$	Discharging UA coefficient 2	-1.419×10^5	$\frac{\mathrm{W}}{\mathrm{K}}$
$c_{\text{dchrg},3}$	Discharging UA coefficient 3	9.366×10^4	$\frac{\mathrm{W}}{\mathrm{K}}$

5.2 Validation of the Ice Tank Model

Figures 10-13 show the performance of the ice tank model (orange) against the experimental data (blue) for the tested charge and discharging conditions following the strategy of holding the inlet temperature, $T_{in}\mathrm{Exp}$, constant. The top plot shows the outlet temperatures, T_{out}, the second plot shows the cumulative heat transfer, the third shows the error in the cumulative heat transfer, and the bottom plot shows the SOC. The SOC of the model does not account for sensible cooling of the ice and so does not have negative values as the experimental lines do.

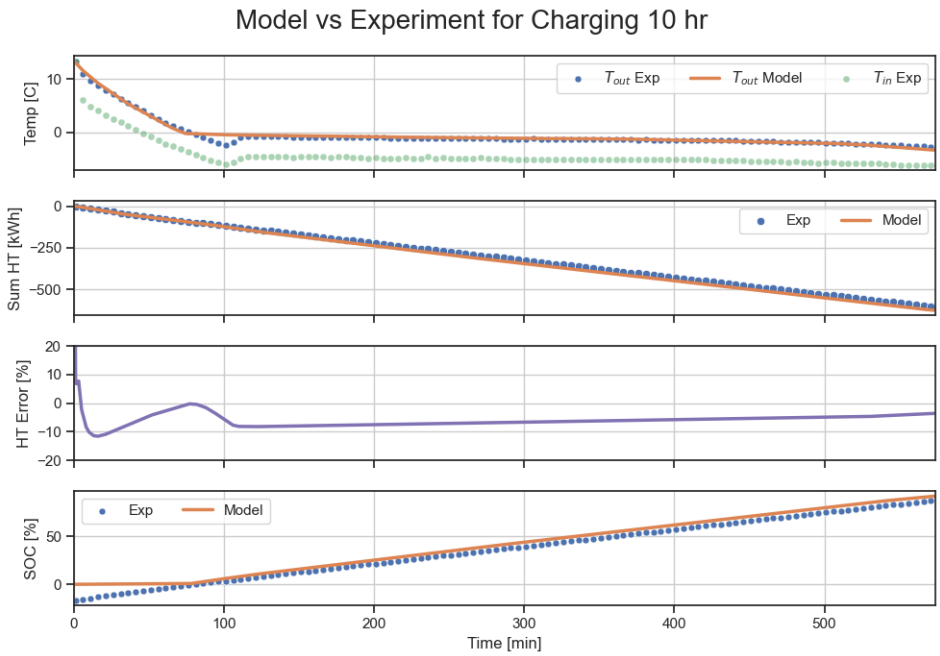

Figure 10: Validation of the ice tank model for 0.11C charge

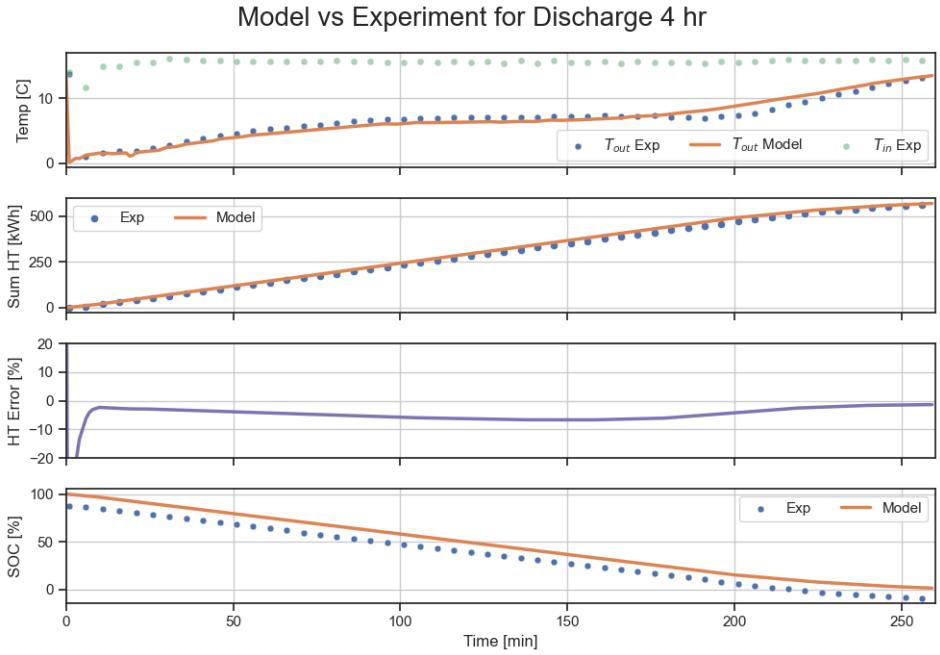

Figure 11: Validation of the ice tank model for 0.25C discharge

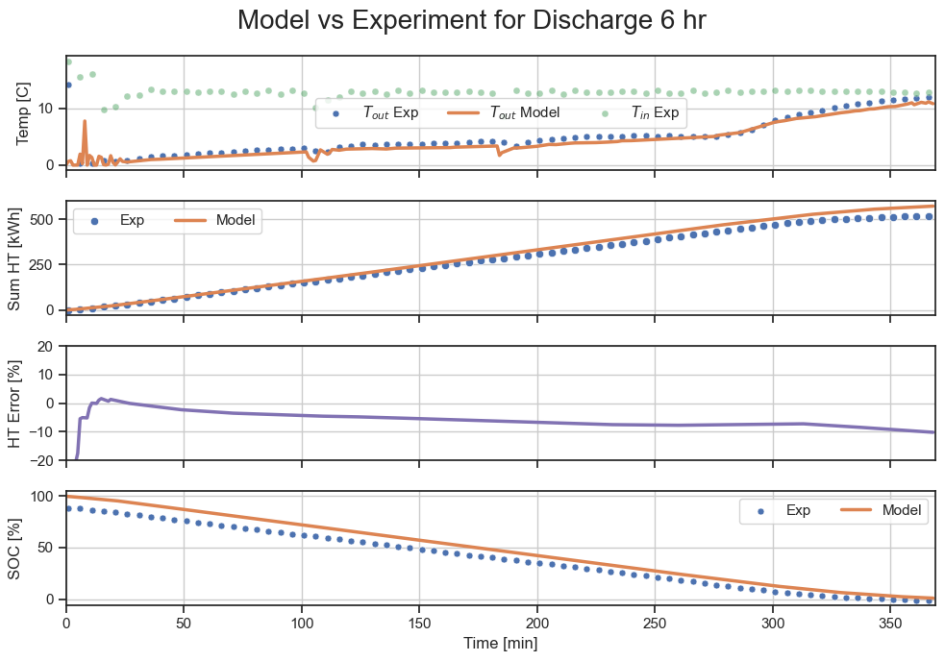

Figure 12: Validation of the ice tank model for 0.167C discharge

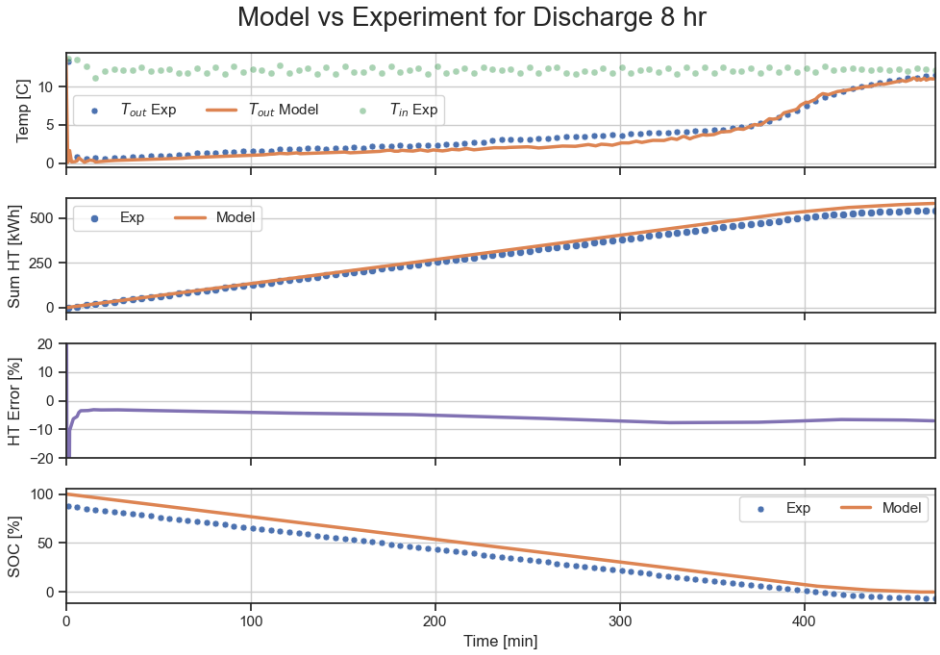

Figure 13: Validation of the ice tank model for 0.125C discharge

5.3 Utility Rates for the Three Locations

5.3.1 San Diego Gas and Electric AL TOU2 Secondary

The monthly demand for this utility is $52.83/kW. From 4:00 PM until 9:00 PM, for June through October, there is a TOU demand adder of $26.81/kW, and for the rest of the year there is a TOU demand adder of $1.12/kW. The demand rate is the same for weekdays and weekends.

There are six different energy charges for this utility rate. From 4:00 PM until 9:00 PM, for both weekends and weekdays, the energy charge is $0.16869/kWh for June through October and $0.19708/kWh for all other months. From 9:00 PM through 11:00 PM, for both weekends and weekdays the energy charge is $0.10133/kWh for June through October and $0.11384/kWh for all other months. The cost is also $0.10133/kWh for June through October from 6:00 AM to 4:00 PM on weekdays and from 2:00 PM to 4:00 PM on weekends. The cost is also $0.11384/kWh for all other months from 6:00 AM to 4:00 PM on weekdays and from 2:00 PM to 4:00 PM on weekends, except March and April from 10:00 AM to 2:00 PM, where the cost is $0.08971/kWh. The cost is $0.09788/kWh for June through October from 12:00 AM to 6:00 AM on weekdays and from 12:00 AM to 2:00 PM on weekends and $0.08971/kWh for all other months. The rate is illustrated in Figure 14(a) for demand and Figure 14(b) for energy.

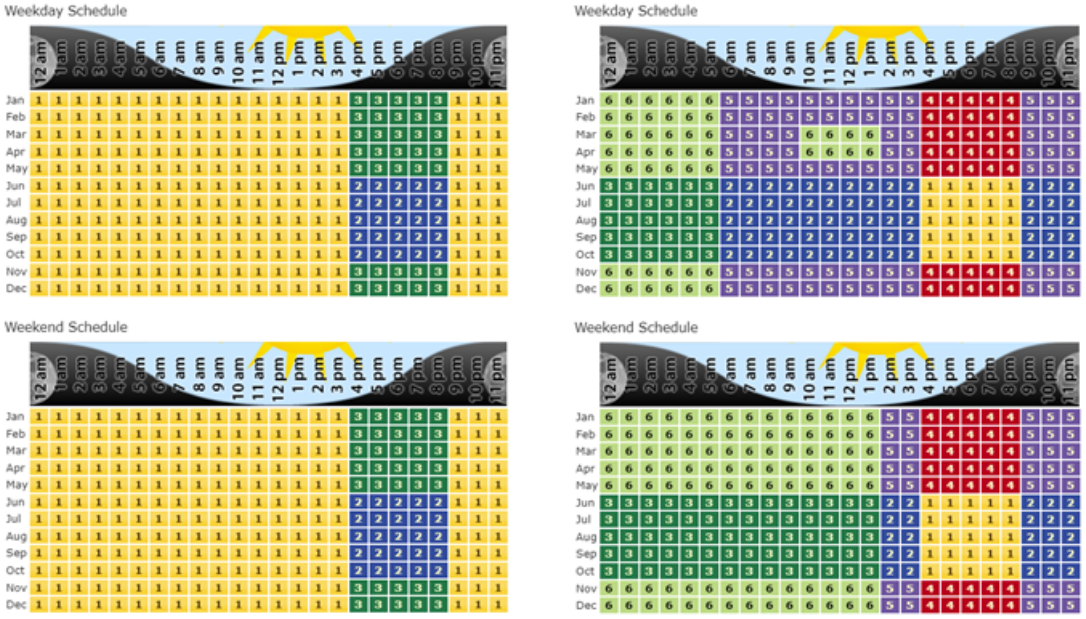

(a) (b)

Figure 14: San Diego Utility Rates

5.3.2 Nevada Power Company ME OLGS 1 TOU

The monthly demand for this utility is $3.68/kW. From 1:00 PM until 7:00 PM, for all days in June through September, there is a TOU demand adder of $7.60/kW. For all days and hours outside of June through September, there is a TOU demand adder of $0.26/kW.

For all days in June through September, the energy charge is $0.1795/kWh from 1:00 PM until 7:00 PM and $0.07636/kWh otherwise. For all days and hours outside of June through September, the energy charge is $0.07534/kWh. The rate is illustrated in Figure 15(a) for demand and Figure 15(b) for energy.

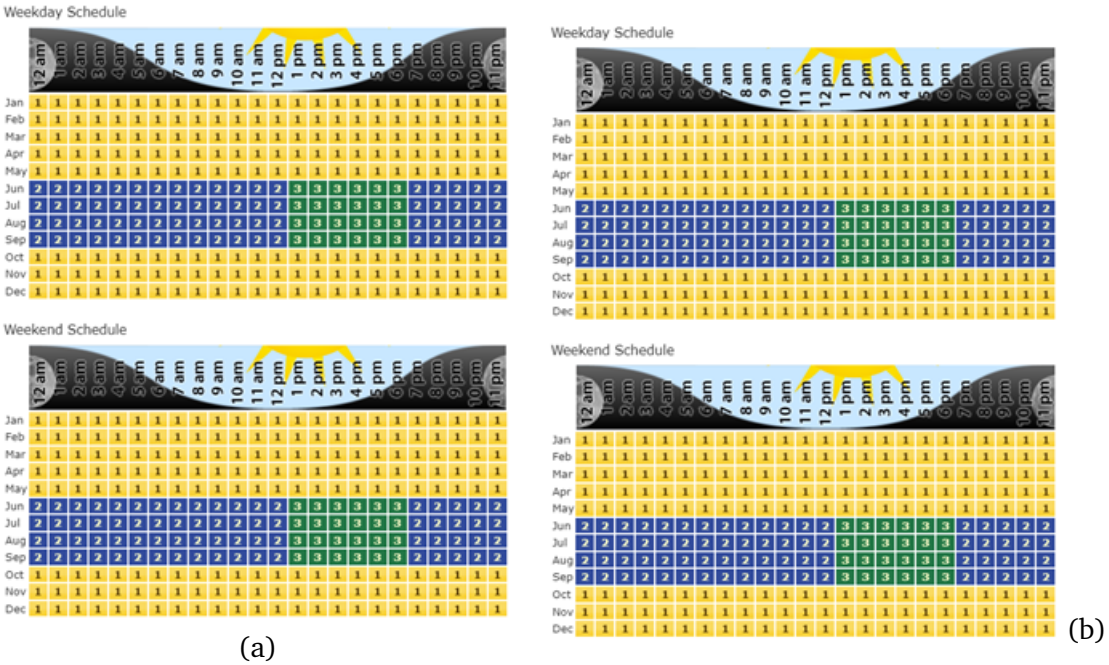

(a) (b)

Figure 15: Las Vegas Utility Rates

5.3.3 El Paso Electric Company General Service Rate—TOU Secondary Voltage

The monthly demand for this utility is $24.5/kW from June through September and $20.37/kW for all other months.

On weekdays in June through September from 12:00 PM to 6:00 PM the energy charge is $0.133865/kWh and $0.020275/kWh otherwise. The rate is illustrated in Figure 16(a) for demand and Figure 16(b) for energy.

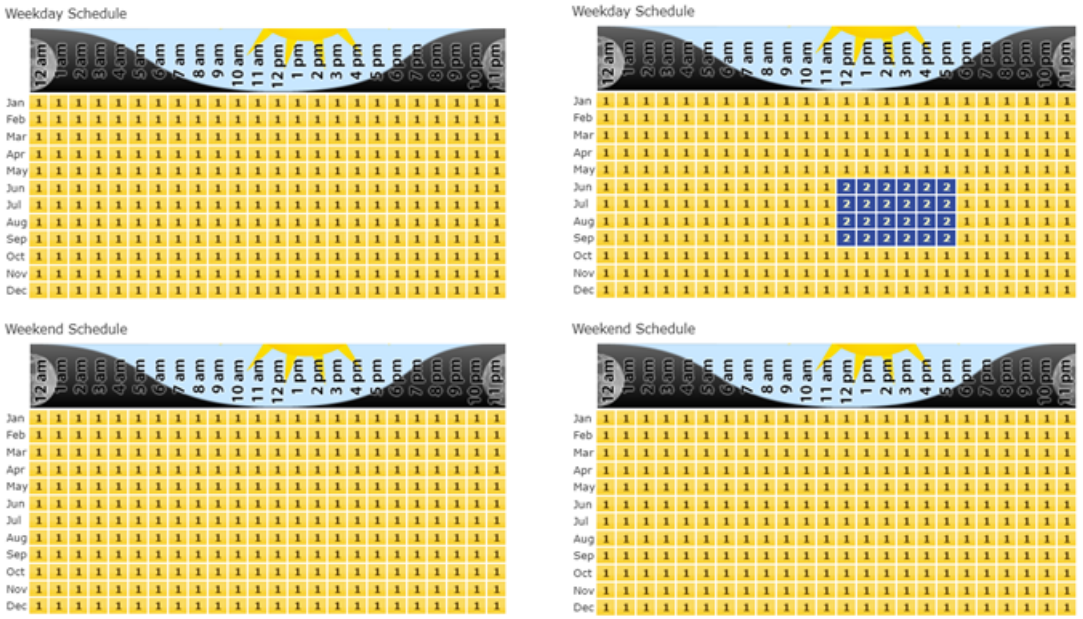

(a) (b)

Figure 16: El Paso Utility Rates

5.4 Schedule Controls for San Diego and El Paso

Figure 17 shows the schedule for San Diego, where the utility rate has TOU periods for all three seasons. The summer load is very large so during the TOU period, the SOC will be discharged to a much greater extent than in spring and autumn, and so has a much longer charge period. Figure 18 shows that the schedule for El Paso is the same across all three seasons and discharges across the occupancy hours since there is no TOU.

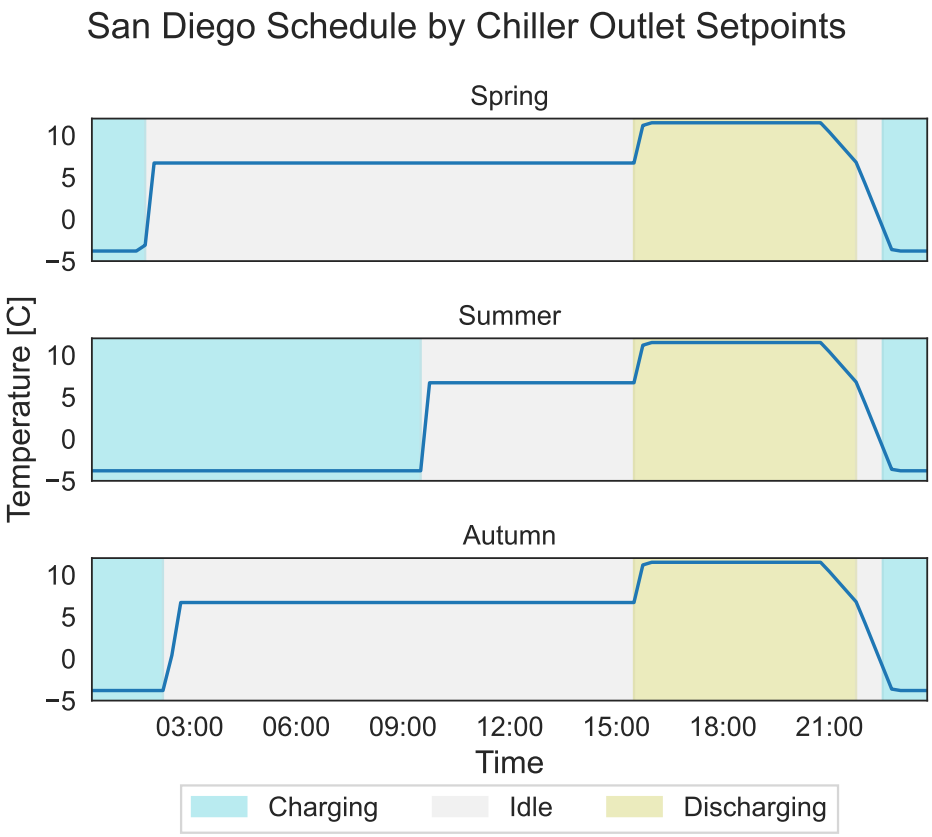

Figure 17: Schedule-based controls for San Diego, California

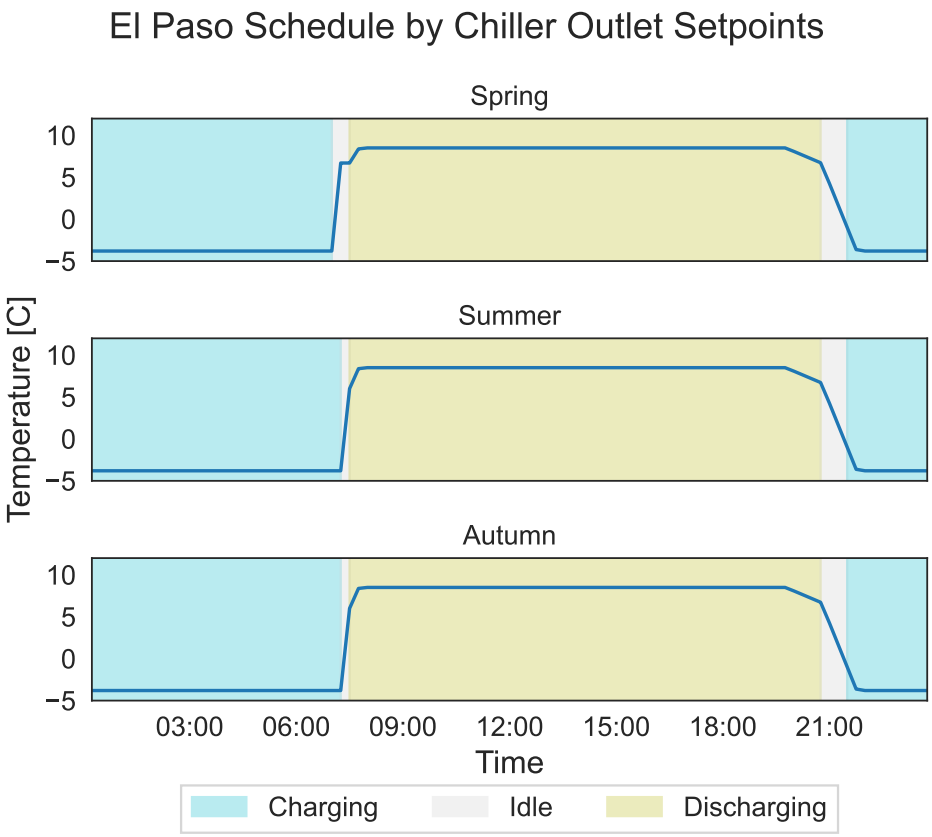

Figure 18: Schedule-based controls for El Paso, Texas

5.5 Optimization Model

5.5.1 Parameters and Variables

The ice tank parameters are the same as for the Python ice tank model in Section 2.1.1, listed in Table 2, and are constant throughout all simulations.

The parameters for the rest of the system are listed in Table 3 which includes time series forecasts, chiller regression coefficients, and utility rate costs that are updated for each control problem.

Table 3: System parameter values

Parameter	Definition	Value
Δt	Time interval	900 s
$\dot{m}_{\text{brnch}}$	Mass flow rate of chiller water branch	4.4963
M_{tank}	Mass of fluid in tank	6253.732
$C_{p,\text{ice}}$	Heat capacity of ice	2030
$C_{p,\text{wtr}}$	Heat capacity of water	4207
H	Enthalpy of melting for ice	334000
ϵ_{tank}	Tank temperature curve epsilon	
$T_{\text{tank,min}}$	Minimum tank temperature	-10 C
$T_{\text{tank,max}}$	Maximum tank temperature	20 C
S_{min}	Minimum tank state of charge	0.025
S_{max}	Maximum tank state of charge	0.99
T_{env}	Temperature of environment	20 C
U_{env}	Tank heat exchange with environment	
T^t_{cond}	Temperature of condenser inlet	
$T^t_{\Delta\text{load}}$	Temperature increase of the chiller water due to building load	
$c^t_{\text{chlr},0}$	Chiller power function regression coefficient 0	
$c^t_{\text{chlr},1}$	Chiller power function regression coefficient 1	
P^t_{load}	Non-thermal load of the building at time t	$\mathcal{R}^+$
P^t_{pv}	Power generated by PV at time t	$\mathcal{R}^+$
$\mathcal{P}$	Set of all TOU periods in electricity bill	$\mathcal{I}$
$B_{\text{dmp},p}$	TOU demand cost for period p	$\mathcal{R}^+$
B_{dmm}	Monthly demand cost for period p	$\mathcal{R}^+$
$B_{\text{enr},t}$	TOU energy cost for time t	$\mathcal{R}^+$
B_{01}	Cost hyperparameter for binary penalty	$\mathcal{R}^+$
B_{Δ}	Cost hyperparameter for regularizing max difference	$\mathcal{R}^+$
B_{∇}	Cost hyperparameter for regularizing first derivative	$\mathcal{R}^+$
B_{∇^2}	Cost hyperparameter for regularizing second derivative	$\mathcal{R}^+$

The system variables to be optimized are shown in Table 4, which includes temperatures, SOC, mass flow rates, charge or discharge rate, and power flow variables that determine demand and energy components of the utility bill.

Table 4: System variables

Symbol	Definition	Value
$\mathcal{T}$	Set of all 15-min time steps	$[0, 96]$
Q^t_{tank}	Available heat in tank at time t	$\mathcal{R}^+$
T^t_{tank,d_1}	Tank temperature continuous var 1 at time t	$[0, -\epsilon - T_{\text{tank,min}}]$
T^t_{tank,d_2}	Tank temperature continuous var 2 at time t	$[0, 2\epsilon]$
T^t_{tank,d_3}	Tank temperature continuous var 3 at time t	$[0, T_{\text{tank,max}} - \epsilon]$
T^t_{tank,b_1}	Tank temperature binary var 1 at time t	$0, 1$
T^t_{tank,b_2}	Tank temperature binary var 2 at time t	$0, 1$
T^t_{tank}	Tank temperature at time t	$[T_{\text{tank,min}}, T_{\text{tank,max}}]$
S^t	Tank state of charge at time t	$[0, 1]$
$T^t_{\text{tank, in}}$	Tank inlet temperature at time t	$[T_{\text{tank,min}}, T_{\text{tank,max}}]$
$T^t_{\text{tank, out}}$	Tank outlet temperature at time t	$[T_{\text{tank,min}}, T_{\text{tank,max}}]$
$T^t_{\text{brnch, in}}$	Chilled water branch outlet temperature at time t	$[T_{\text{tank,min}}, T_{\text{tank,max}}]$
$T^t_{\text{brnch, out}}$	Chilled water branch outlet temperature at time t	$[T_{\text{tank,min}}, T_{\text{tank,max}}]$
$\dot{m}^t_{\text{tank}}$	Mass flow rate of chilled water flowing through tank at time t	$[0, \dot{m}_{\text{brnch}}]$
I^t_{chrg}	Indicates tank is charging at time t	$0, 1$
$C^t_{p,\text{brn}}$	Heat capacity of brine at time t	$\mathcal{R}^+$
$\bar{C}^t_{p,\text{brn}}$	Average heat capacity of brine at time t	$\mathcal{R}^+$
$U^t_{\text{brn,chrg}}$	Tank heat exchange with brine when charging at time t	$[0, 1]$
$U^t_{\text{brn,dchrg}}$	Tank heat exchange with brine when discharging at time t	$[0, 1]$
U^t_{brn}	Tank heat exchange with brine	$[0, 1]$
E^t_{brn}	Tank heat exchange effectiveness with brine at time t	$[0, 1]$
$U^t_{\text{brnch,chrg}}$	Tank heat exchange at outlet at time t	$[0, 1]$
$U^t_{\text{brnch,dchrg}}$	Tank heat exchange at outlet at time t	$[0, 1]$
U^t_{brnch}	Tank heat exchange at outlet	$[0, 1]$
E^t_{brnch}	Tank heat exchange effectiveness at outlet at time t	$[0, 1]$
$Q^t_{\text{brn,max}}$	Max heat exchange with brine at time t	$\mathcal{R}^+$
Q^t_{brn}	Actual heat exchange with brine at time t	$\mathcal{R}^+$
Q^t_{env}	Heat exchange with environment at time t	$\mathcal{R}^+$
Q^t_{total}	Total tank heat exchange at time t	$\mathcal{R}^+$
Q^t_{tank}	Available heat in tank at time t	$\mathcal{R}^+$
P^t_{chlr}	Power consumption of the chiller at time t	$\mathcal{R}^+$
P^t_{buy}	Power purchased from the grid at time t	$\mathcal{R}^+$
P^t_{sell}	Power sold to the grid at time t	$\mathcal{R}^+$
D^p	TOU demand for period p in current month	$\mathcal{R}^+$
D	Monthly demand for current month	$\mathcal{R}^+$

5.5.2 Tank Temperature

The energy available in the tank depends on the temperature and is determined across the phase change using a piecewise model for the different heat capacities of ice and water:

$$\forall\, t \in \mathcal{T}, \quad T^t_{\text{tank}} = T^t_{\text{tank},d_1} + T^t_{\text{tank},d_2} + T^t_{\text{tank},d_3} + T_{\text{tank,min}} \tag{10a}$$

$$\forall\, t \in \mathcal{T}, \quad S^t = 1 - \frac{T^t_{\text{tank},d_2}}{2\epsilon} \tag{10b}$$

$$\forall\, t \in \mathcal{T}, \quad T^t_{\text{tank},b_1}(\epsilon - T_{\text{tank,min}}) \leq T^t_{\text{tank},d_1} \tag{10c}$$

$$\forall\, t \in \mathcal{T}, \quad T^t_{\text{tank},d_1} \leq -\epsilon - T_{\text{tank,min}} \tag{10d}$$

$$\forall\, t \in \mathcal{T}, \quad 2\epsilon T^t_{\text{tank},b_2} \leq T^t_{\text{tank},d_2} \tag{10e}$$

$$\forall\, t \in \mathcal{T}, \quad T^t_{\text{tank},d_2} \leq 2\epsilon T^t_{\text{tank},b_1} \tag{10f}$$

$$\forall\, t \in \mathcal{T}, \quad T^t_{\text{tank},d_3} \leq T^t_{\text{tank},b_2}(T_{\text{tank,max}} - \epsilon) \tag{10g}$$

$$\forall\, t \in \mathcal{T}, \quad Q^t_{\text{tank}} = M_{\text{tank}}(C_{p,\text{ice}} T^t_{\text{tank},d_1} + \frac{T^t_{\text{tank},d_2} H}{2\epsilon} + C_{p,\text{wtr}} T^t_{\text{tank},d_3}) \tag{10h}$$

Equation 10a calculates the temperature of the tank as the sum of the piecewise temperatures, where the segments are ice, phase change, and water, respectively. Eq 10b calculates the SOC based on the amount of ice: $S = 0$ is all water regardless of water temperature and $S = 1$ is all ice regardless of ice temperature. Eq 10c-10g set the lower and upper bounds for the segments of the piecewise temperature function, with an $\epsilon = 0.01$ around the phase change temperature to avoid a segment with an infinite slope. Eq 10h calculates the available heat from the temperature of the tank.

5.5.3 Heat Transfer

The temperature of the tank depends on heat transfer from the environment and from the brine fluid of the chilled water loop. The effectiveness of heat transfer during charging or discharging is modulated by the SOC. The equations are as follows:

$$\forall\, t \in \mathcal{T}, \quad I^t_{\text{chrg}} - (S^t - S^{t-1}) \geq 0 \tag{11a}$$

$$\forall\, t \in \mathcal{T}, \quad (1 - I^t_{\text{chrg}}) + (S^t - S^{t-1}) \geq 0 \tag{11b}$$

$$\forall\, t \in \mathcal{T}, \quad C^t_{p,\text{brn}} = 2.725 T^t_{\text{tank, in}} + 3058.208 \tag{11c}$$

$$\forall\, t \in \mathcal{T}, \quad \bar{C}^t_{p,\text{brn}} = 2.725 \frac{T^t_{\text{tank, in}} + T^{t-1}_{\text{tank}}}{2} + 3058.208 \tag{11d}$$

$$\forall\, t \in \mathcal{T}, \quad U^t_{\text{brn,chrg}} = c_{\text{chrg},0} + c_{\text{chrg},1} S^{t-1} + c_{\text{chrg},2}(S^{t-1})^2 + c_{\text{chrg},3}(S^{t-1})^3 \tag{11e}$$

$$\forall\, t \in \mathcal{T}, \quad U^t_{\text{brn,dchrg}} = c_{\text{dchrg},0} + c_{\text{dchrg},1} S^{t-1} + c_{\text{dchrg},2}(S^{t-1})^2 + c_{\text{dchrg},3}(S^{t-1})^3 \tag{11f}$$

$$\forall\, t \in \mathcal{T}, \quad U^t_{\text{brn}} = U^t_{\text{brn,dchrg}}(1 - I^t_{\text{chrg}}) + U^t_{\text{brn,chrg}} I^t_{\text{chrg}} \tag{11g}$$

$$\forall\, t \in \mathcal{T}, \quad E^t_{\text{brn}} = 1 - \exp \frac{-U^t_{\text{brn}}}{\dot{m}^t_{\text{tank}} C^t_{p,\text{brn}}} \tag{11h}$$

$$\forall\, t \in \mathcal{T}, \quad Q^t_{\text{brn,max}} = \dot{m}^t_{\text{tank}} \bar{C}^t_{p,\text{brn}}(T^t_{\text{tank, in}} - T^{t-1}_{\text{tank}})\Delta t \tag{11i}$$

$$\forall\, t \in \mathcal{T}, \quad Q^t_{\text{brn}} = Q^t_{\text{brn,max}} E^t_{\text{tank}} \tag{11j}$$

$$\forall\, t \in \mathcal{T}, \quad Q^t_{\text{env}} = U_{\text{env}}(T^t_{\text{env}} - T^{t-1}_{\text{tank}})\Delta t \tag{11k}$$

$$\forall\, t \in \mathcal{T}, \quad Q^t_{\text{total}} = Q^t_{\text{brn}} + Q^t_{\text{env}} \tag{11l}$$

$$\forall\, t \in \mathcal{T}, \quad Q^t_{\text{tank}} = Q^{t-1}_{\text{tank}} + Q^t_{\text{total}} \tag{11m}$$

$$\tag{11n}$$

Equations 11a and 11b calculates the charging mode of the tank as whether or not the SOC is increasing. Eq 11c and 11d calculate heat capacities of the brine based on a linear regression but at the tank inlet and

as the average across the tank, respectively. Eq 11e-11h calculates the heat transfer effectiveness of the tank with the brine at the inlet based on the previous SOC using regression coefficients depending on whether the tank is charging and discharging. Eq 11i calculates the max heat transfer with the brine across the tank while 11j is the effective heat transfer. Eq 11k is the heat transfer with the environment through the tank surface and Eq 11l is the total heat transfer. The temperature of the tank is then updated using the total heat transfer in Eq 11m.

5.5.4 Chilled Water Loop Outlet Temperature

The outlet of the tank mixes with the bypass flow to form the outlet of the branch, which then flows across the demand side of the building. The mass flow rate of the chilled water loop is constant and so the temperature rise of the brine across the building is used as a proxy for the thermal load. There are separate but structurally identical effectiveness terms for the heat transfer across the branch.

$$\forall\, t \in \mathcal{T}, \quad U^t_{\text{brnch,chrg}} = c_{\text{chrg},0} + c_{\text{chrg},1} S^t + c_{\text{chrg},2}(S^t)^2 + c_{\text{chrg},3}(S^t)^3 \tag{12a}$$

$$\forall\, t \in \mathcal{T}, \quad U^t_{\text{brnch,dchrg}} = c_{\text{dchrg},0} + c_{\text{dchrg},1} S^t + c_{\text{dchrg},2}(S^t)^2 + c_{\text{dchrg},3}(S^t)^3 \tag{12b}$$

$$\forall\, t \in \mathcal{T}, \quad U^t_{\text{brnch}} = U^t_{\text{brnch,dchrg}}(1 - I^t_{\text{chrg}}) + U^t_{\text{brnch,chrg}} I^t_{\text{chrg}} \tag{12c}$$

$$\forall\, t \in \mathcal{T}, \quad E^t_{\text{brnch}} = 1 - \exp \frac{-U^t_{\text{brnch}}}{\dot{m}^t_{\text{tank}} C^t_{p,\text{brn}}} \tag{12d}$$

$$\forall\, t \in \mathcal{T}, \quad T^t_{\text{tank, out}} = T^t_{\text{tank, in}} - E^t_{\text{brnch}}(T^t_{\text{tank, in}} - T^t_{\text{tank}}) \tag{12e}$$

$$\forall\, t \in \mathcal{T}, \quad T^t_{\text{brnch, out}} = \frac{\dot{m}^t_{\text{tank}} T^t_{\text{tank, out}} + (\dot{m}_{\text{brnch}} - \dot{m}^t_{\text{tank}}) T^t_{\text{tank, in}}}{\dot{m}_{\text{brnch}}} \tag{12f}$$

$$\forall\, t \in \mathcal{T}, \quad T^t_{\text{brnch, in}} = T^{t-1}_{\text{brnch, out}} + T^t_{\Delta\text{load}} \tag{12g}$$

$$\forall\, t \in \mathcal{T}, \quad P^t_{\text{chlr}} = c^t_{\text{chlr},0} T^t_{\text{cond}}(T^t_{\text{tank, in}} - T^t_{\text{brnch, in}}) + c^t_{\text{chlr},1}(T^t_{\text{tank, in}} - T^t_{\text{brnch, in}})^2 \tag{12h}$$

$$\forall\, t \in \mathcal{T}, \quad T^t_{\text{tank, in}} \leq T^t_{\text{brnch, in}} \tag{12i}$$

Equations 12a-12d calculate the heat transfer effectiveness of the tank at the branch outlet based on mode and current SOC (the effectiveness of the tank inlet is based on the previous SOC). Eq 12e and 12f determine the temperature of the tank outlet and the temperature of the branch after mixing with the bypass stream, respectively. When the brine flows through the demand side, it warms up across the timestep according to Eq 12g. Upon returning to the supply side, the fluid is cooled by the chiller to the tank inlet temperature using the power calculated by Eq 12h. The chiller is more efficient at lower condenser temperatures and the temperature change across it is constrained to be negative in Eq 12i.

5.5.5 Objective

Periodic boundary conditions for the tank SOC and branch outlet temperature are enough to ensure that the solution is extensible past the 7 day simulation period. Boundary constraints are shown in Equations 13a-13f.

$$\forall\, t \in \mathcal{T}, \quad S^t_{\min} \leq S^t \leq S^t_{\max} \tag{13a}$$

$$\forall\, t \in [1, T], \quad T^t_{\text{tank}} = T^{t+1}_{\text{tank}} \tag{13b}$$

$$\forall\, t \in [1, T], \quad T^t_{\text{brnch, out}} = T^{t+1}_{\text{brnch, out}} \tag{13c}$$

$$\forall\, t \in [1, T], \quad Q^t_{\text{tank}} = Q^{t+1}_{\text{tank}} \tag{13d}$$

$$T^{T}_{\text{brnch, out}} = T^{0}_{\text{brnch, out}} \tag{13e}$$
$$S^{T} = S^{0} \tag{13f}$$

Finally, the optimization problem minimizing the utility bill with binary penalty and derivative regularization is shown below.

$$\min_{P^t_{\text{buy}}, P^t_{\text{sell}}} \quad \sum_{p\in\mathcal{P}} B_{\text{dmp},p} D^p + B_{\text{dmm}} D + \sum_{t\in\mathcal{T}} (P^t_{\text{buy}} - P^t_{\text{sell}}) B_{\text{enr},t} \tag{14}$$
$$+ \sum_{v\in(T_{\text{tank},b_1}, T_{\text{tank},b_2}, I_{\text{chrg}})} B_{01}(-16(v^t - 0.5)^4 + 1)\Big] \tag{15}$$
$$+ \sum_{t\in\mathcal{T}} \Big[\sum_{v\in(T_{\text{tank, in}}, T_{\text{brnch, out}})} B_{\nabla^2}(v^t - 2v^{t-1} + v^{t-2})^2 + B_{\nabla}(v^t - v^{t-1})^2 \tag{16}$$

s.t.
$$D = \max_{p\in\mathcal{P}} D^p \tag{17}$$
$$\forall\, t \in \mathcal{T}, \qquad P^t_{\text{buy}} = P^t_{\text{chlr}} + P^t_{\text{load}} - P^t_{\text{pv}} + P^t_{\text{sell}} \tag{18}$$
$$\forall\, t \in \mathcal{T}, \quad B_{\Delta} \le \Big[(T^t_{\text{tank, in}} - T^t_{\text{brnch, in}}) - (T^{t-1}_{\text{tank, in}} - T^{t-1}_{\text{brnch, in}})\Big]^2 \tag{19}$$

(1a) - (5c)

Equation 14 is the electric bill portion: the first term is the TOU demand charge, the second the monthly demand charge and the third the TOU energy charge, which are summed over each TOU period. As described in 2.4.2, the relaxation of the MINLP to an NLP made solving the problem much more tractable and was supported by penalty terms pushing binary variables toward 0 or 1 in Eq 15. Eq 16 contains the regularization terms to prefer a smooth tank and chiller operation. Eq 17 defines the monthly demand as the max of the TOU demands. Eq 18 balances the purchase and sale of power with the utility. Eq 19 constrains the change in the temperature drop of the chiller between timesteps to reduce ramping. The hyperparameters B_{01}, B_{Δ}, B_{∇} and B_{∇^2} are tuned to balance the costs of the utility with those of binary penalties and max difference, first derivative, and second derivative regularization. The values of these hyperparameters depend on the scaling of the problem and are slightly different per scenario.

5.6 Ice Tank Model Bounds: C-Rates for MPC and Schedule Controls

This section verifies that the ice tank is operated within the C-rate bounds of the model and the experimental data. C-rate is the rate at which the TES is discharged relative to its maximum capacity; a C-rate of 1C is a one-hour full discharge. The operating C-rates are determined by the time window when load is to be reduced, usually the utility rate's TOU period. Figure 19 shows histograms of the operating C-rates of the MPC and schedule across all scenarios.

For the schedule control, a 12-hr discharge for all-day load reduction shows up as the mode around 0.08C. For a 4-hr discharge period, the tank reaches its highest discharge rate of about 0.15C, not reaching the expected 0.25C because the tank is not emptied. The mode around 0.10C is the charging during the 10-hr non-occupancy interval. The MPC appears to operate more often at lower C-rates for both charging and discharging, a sign of small adjustments made to the tank and chiller power. The charging C-rate reaches a higher maximum (0.22C) than for the schedule (0.13C) which happens when the tank is being used for both all-day and peak load reduction, leaving the tank a short window overnight to charge.

The discharge C-rates are within the 0.25C upper bound; however, many discharge C-rates fall below the lower bound of the experiments. Although the UA of the ice tank is a stronger function of C-rate at faster

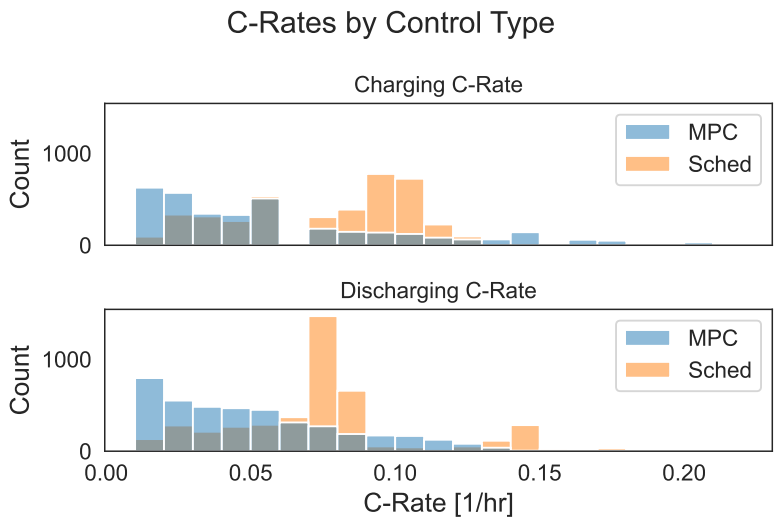

Figure 19: Histogram showing charging and discharging C-rates for MPC and schedule controls

discharge rates because of the impacts of natural convection, the UA should stay relatively constant below C/8 because changes in the resistance are primarily related to conduction [31]. The charging C-rates were at most twice as fast as the experimental 0.11C rate but since the model developed with the experimental data did not require C-rate as a performance factor during discharge, the current charging behavior will be assumed to appropriately extrapolate to around 0.25C. The design of the TES system appears adequate for the scenarios considered.

5.7 Timeseries for Summer Weeks of the Three Locations

Weekends not shown due to low load.

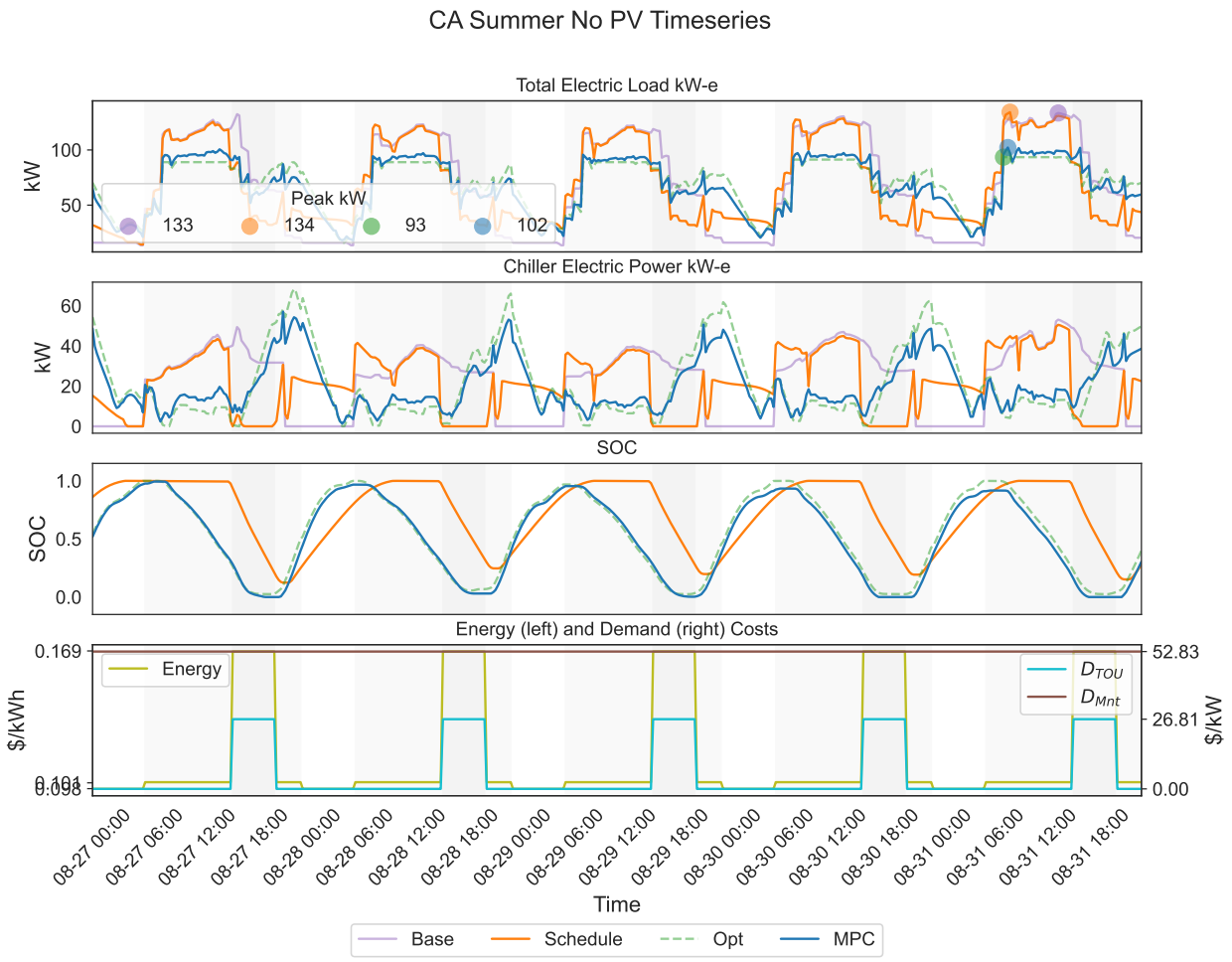

Figure 20: San Diego weekdays of the summer representative week for the No PV case

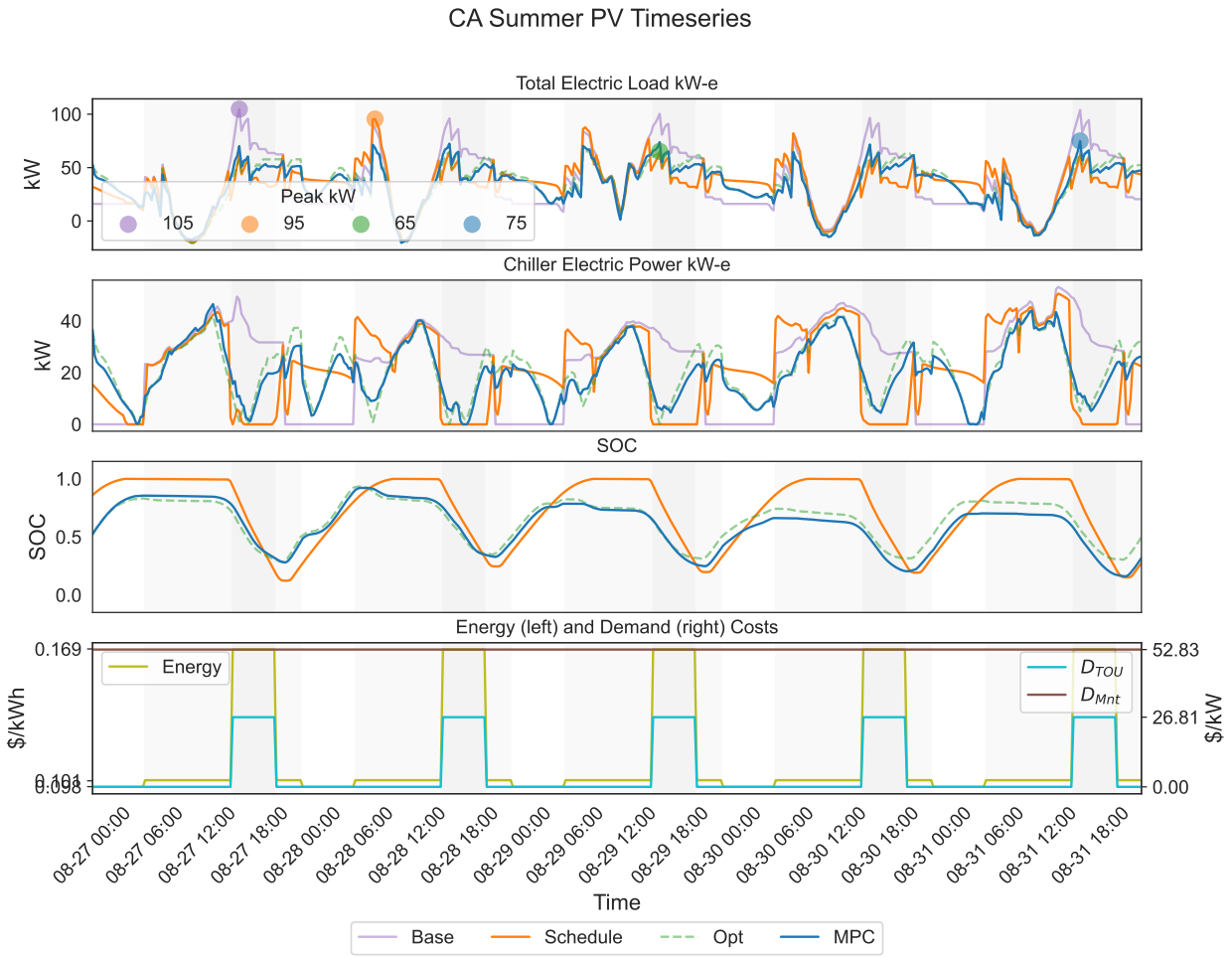

Figure 21: San Diego weekdays of the summer representative week for the PV case

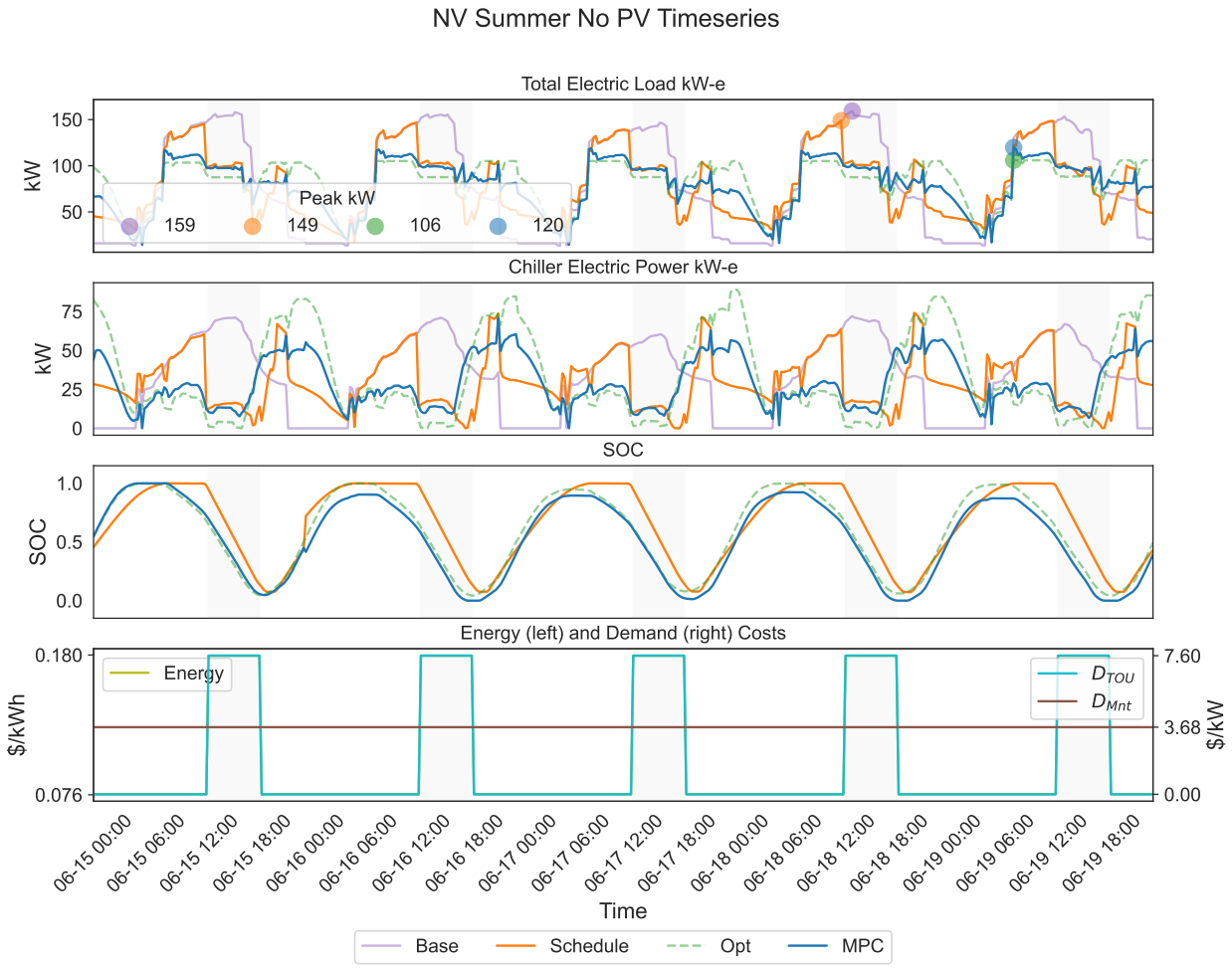

Figure 22: Las Vegas weekdays of the summer representative week for the No PV case

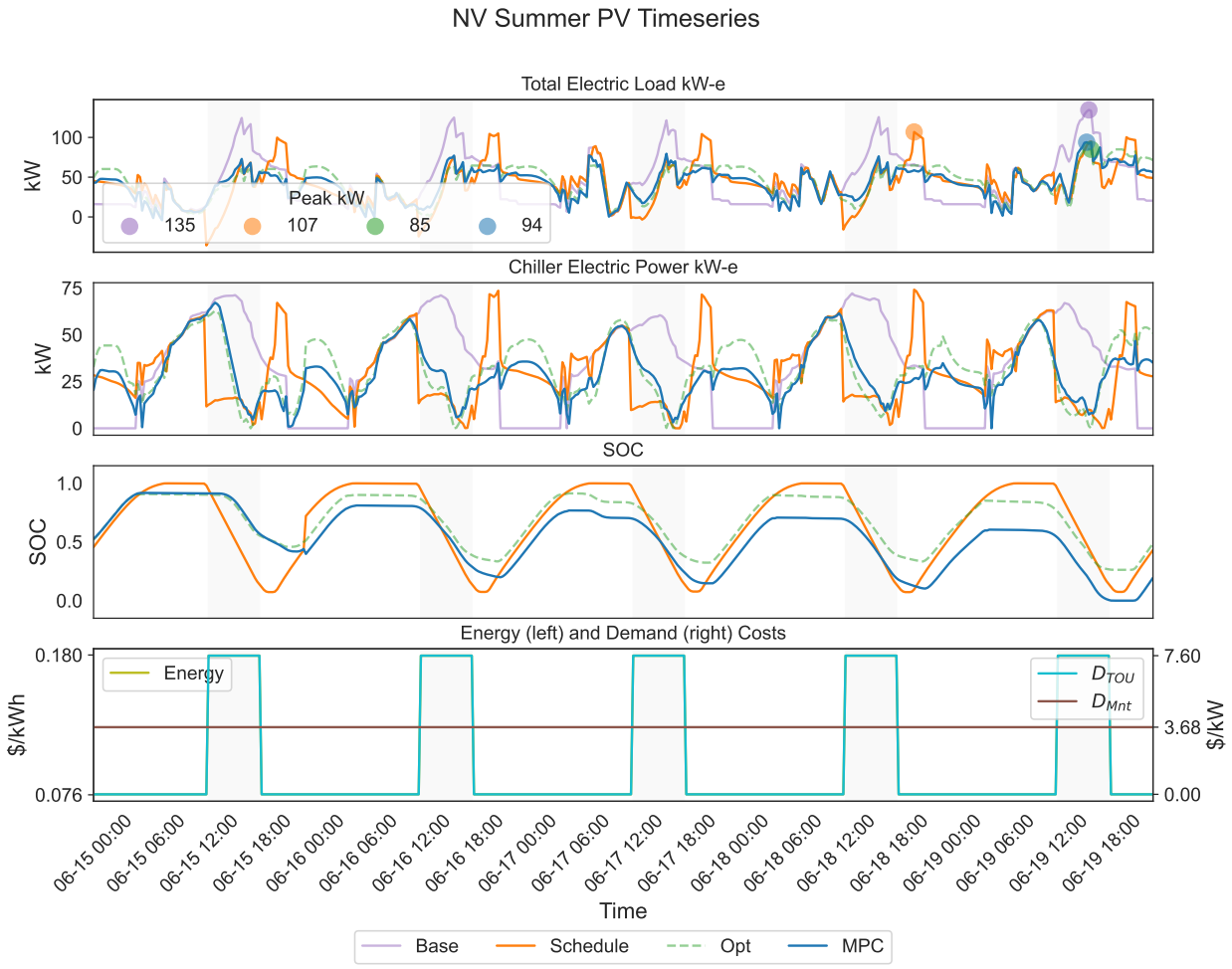

Figure 23: Las Vegas weekdays of the summer representative week for the PV case

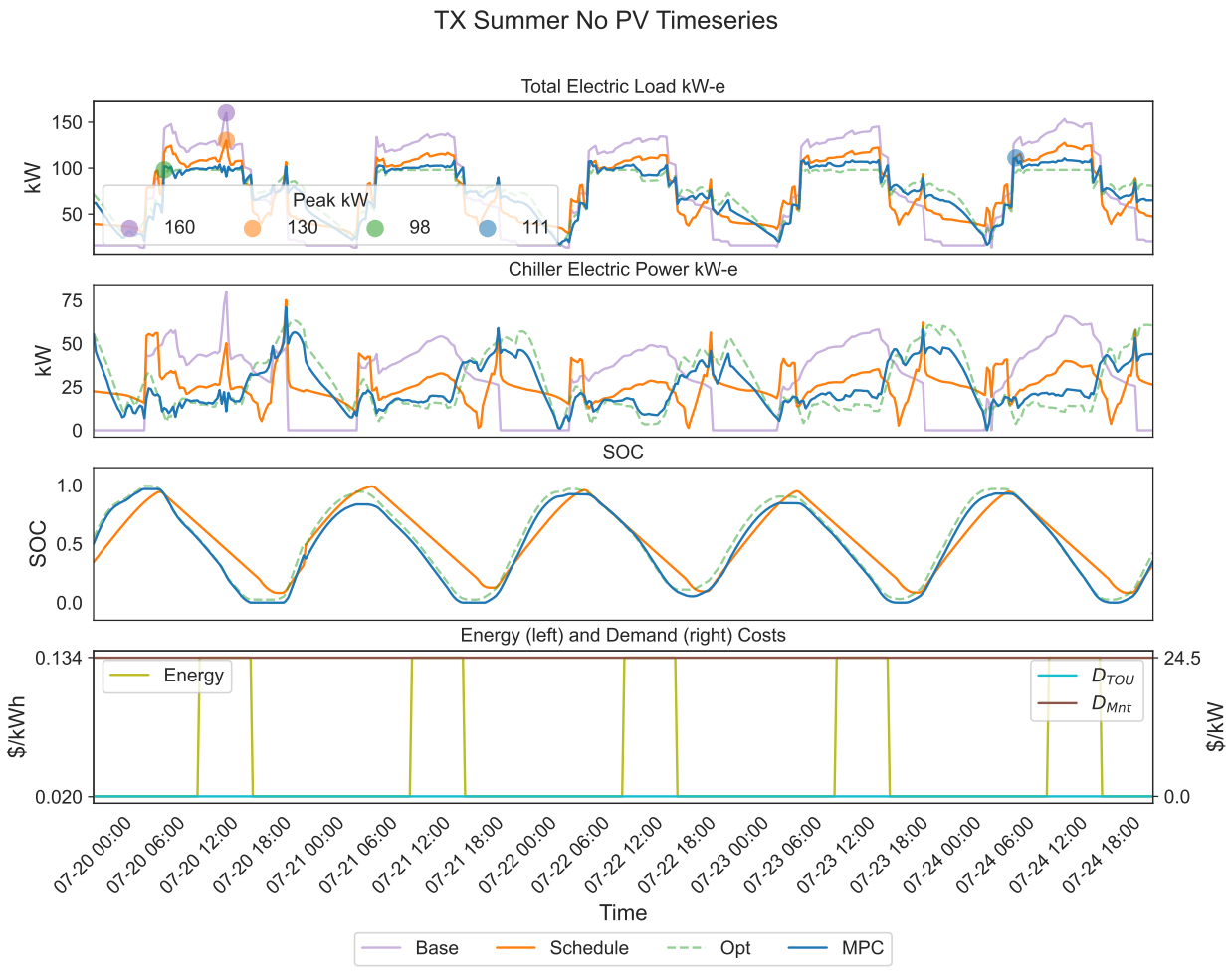

Figure 24: El Paso weekdays of the summer representative week for the No PV case

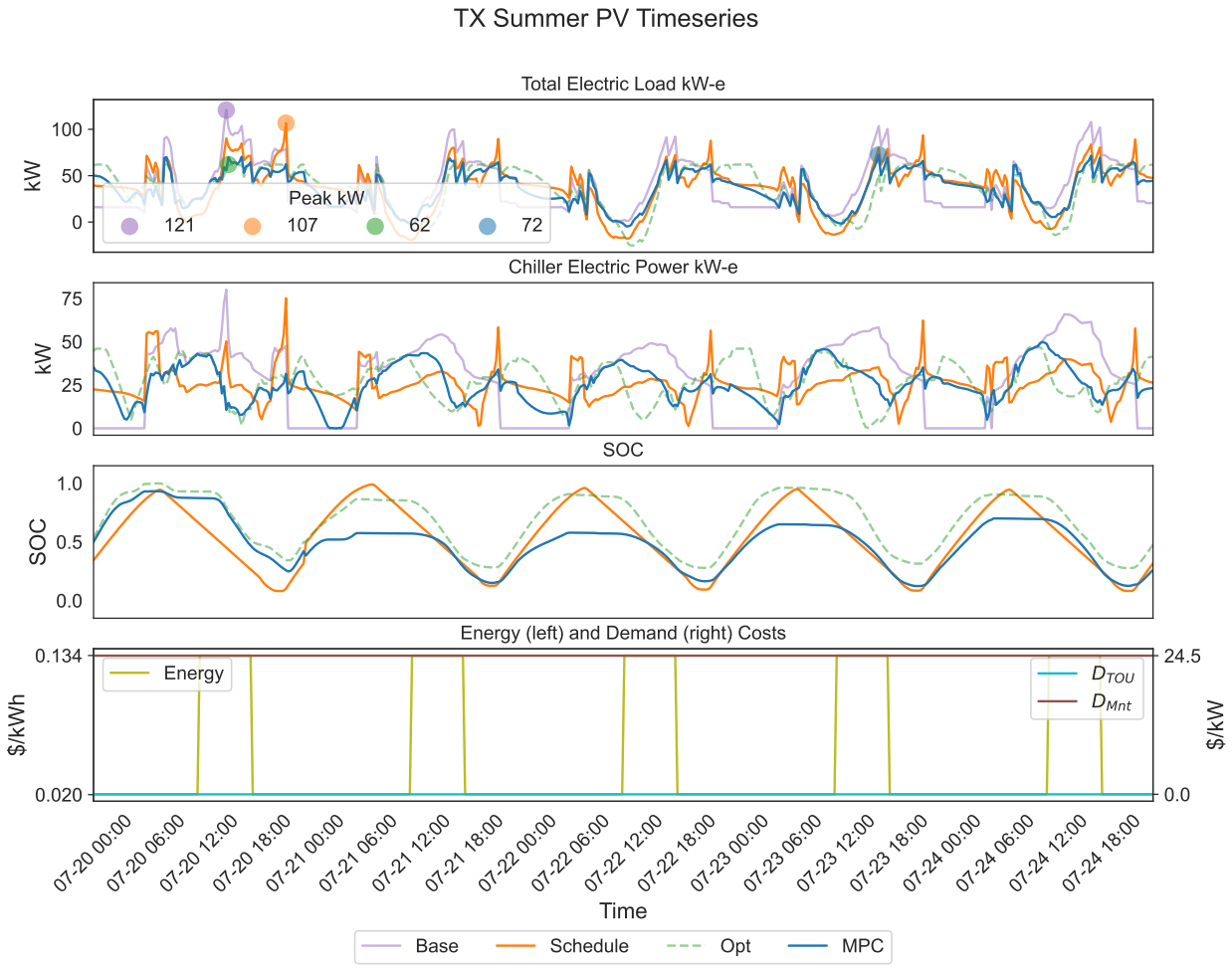

Figure 25: El Paso weekdays of the summer representative week for the PV case

5.8 Savings Breakdown for Las Vegas, NV and El Paso, TX

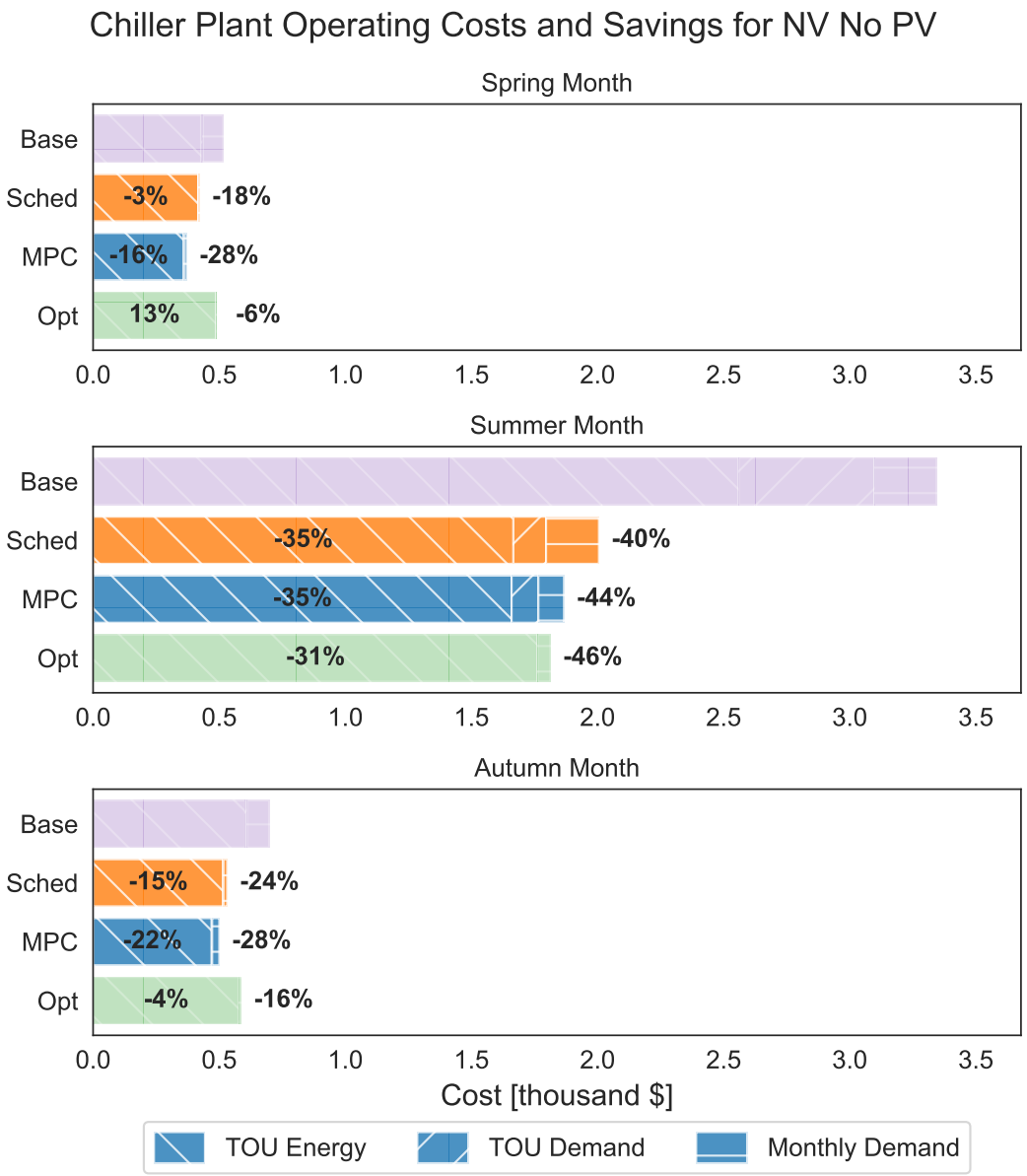

Figure 26: Chiller plant operating cost and savings for the three representative weeks for Las Vegas with no PV

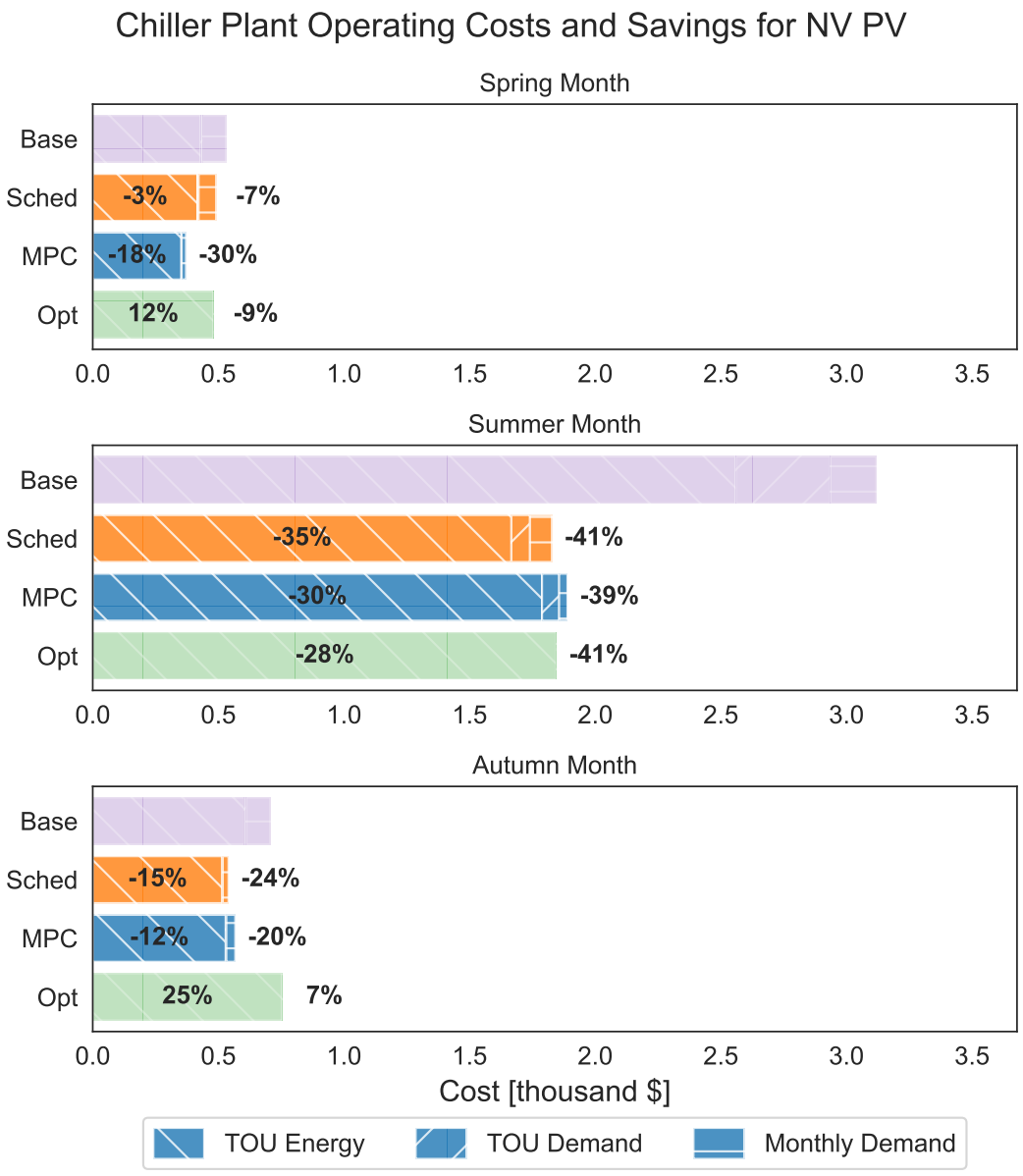

Figure 27: Chiller plant operating cost and savings for the three representative weeks for Las Vegas with PV

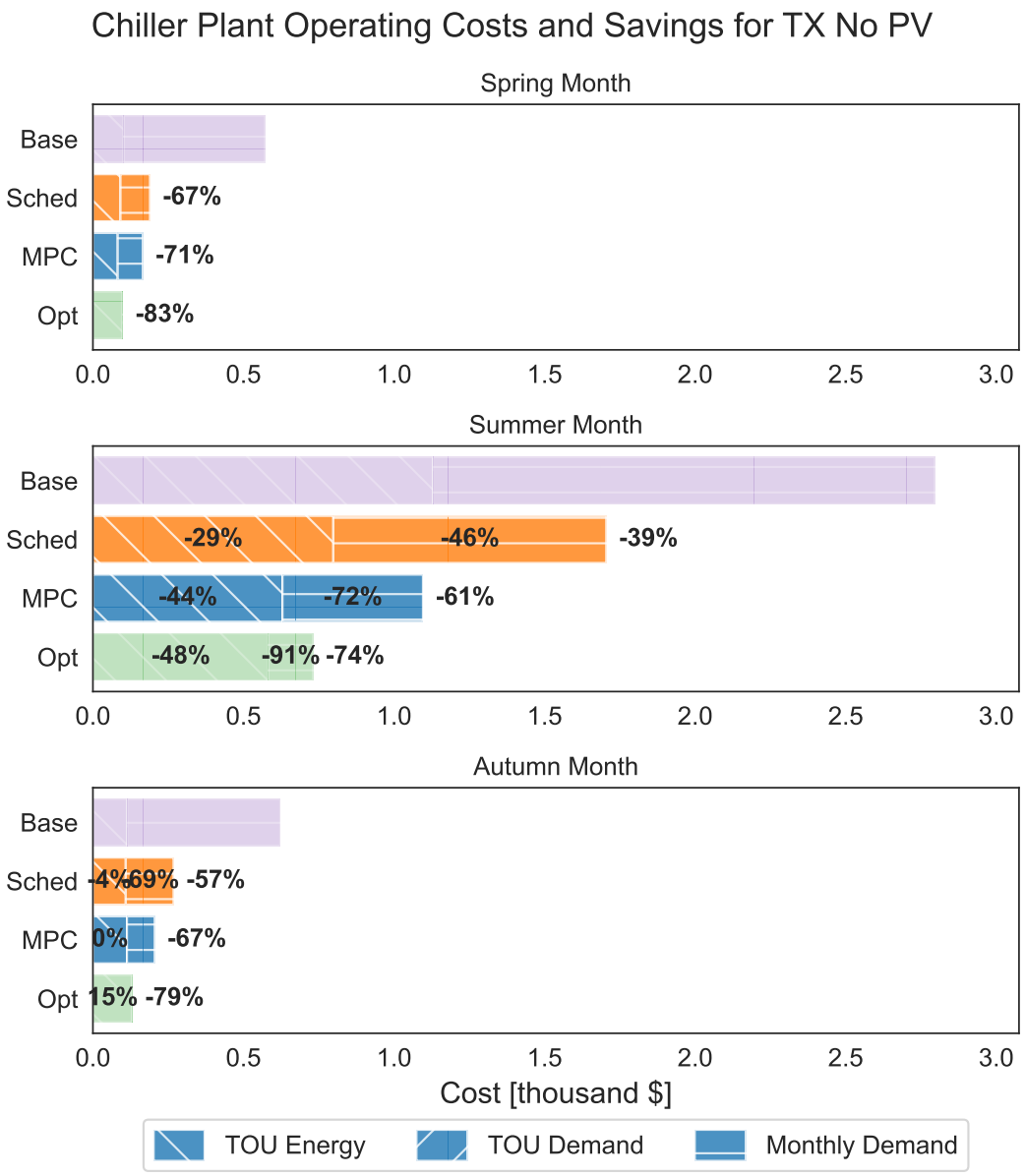

Figure 28: Chiller plant operating cost and savings for the three representative weeks for El Paso with no PV

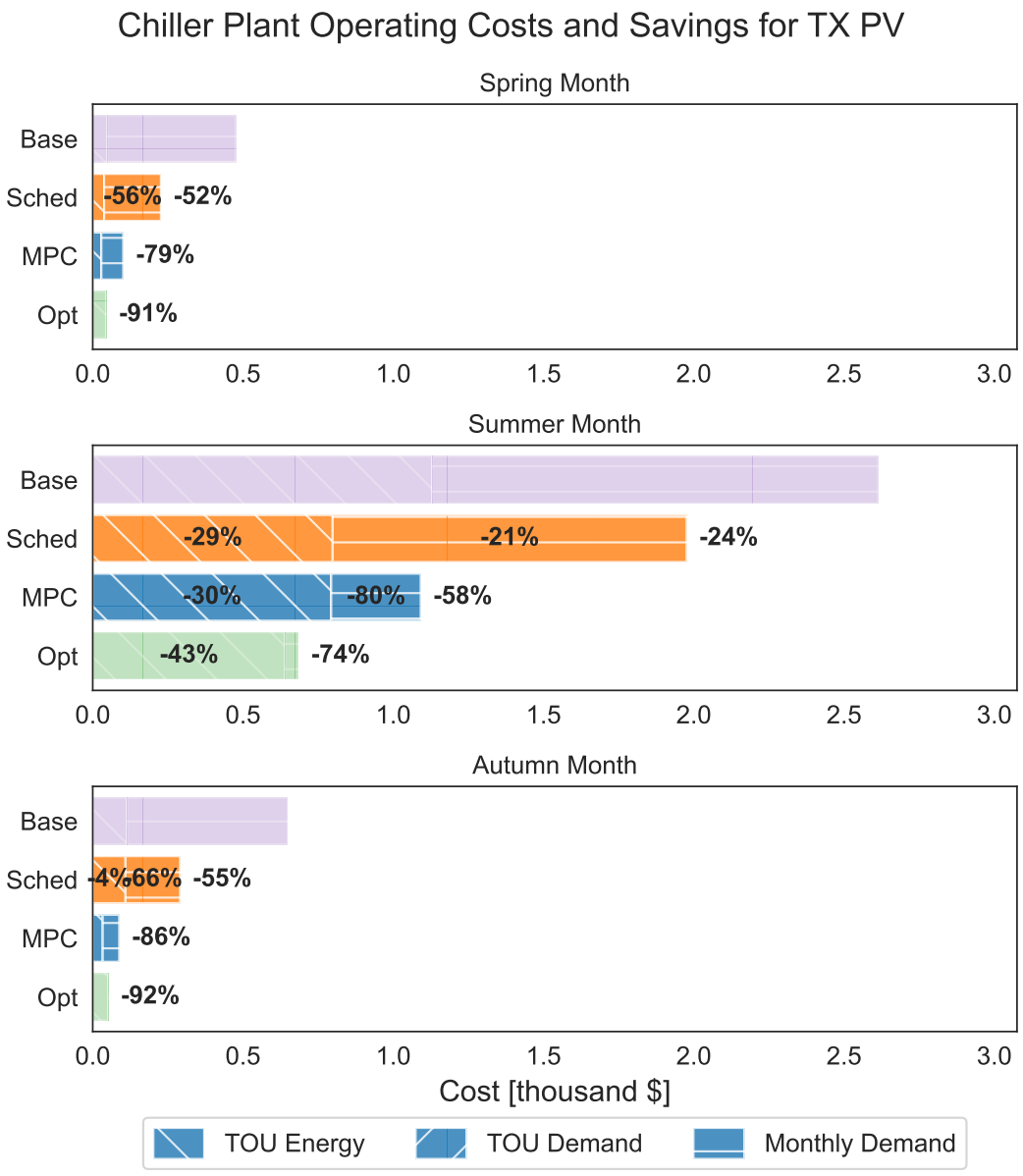

Figure 29: Chiller plant operating cost and savings for the three representative weeks for El Paso with PV

5.9 Total Building Cost Scenario Comparison

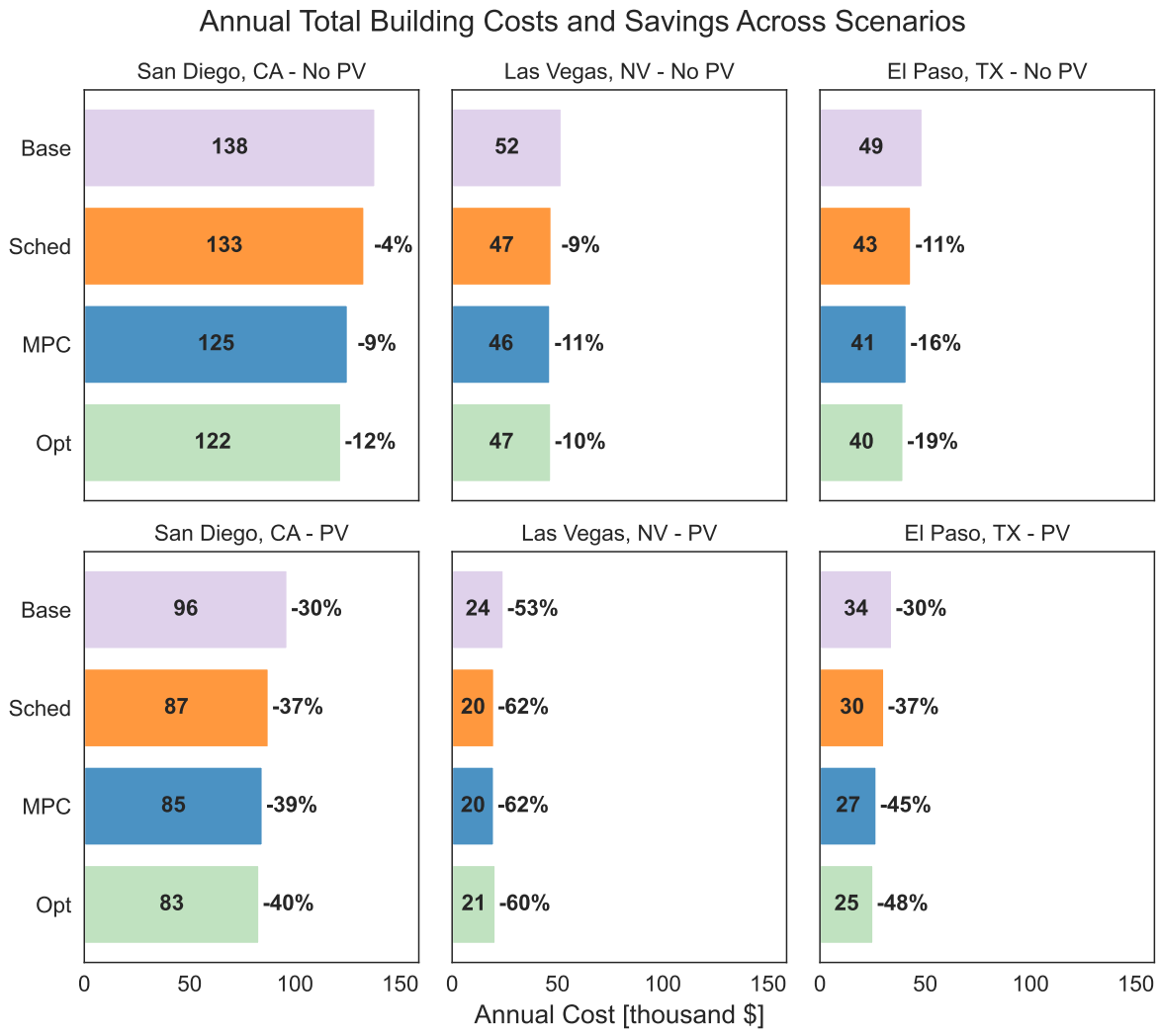

Figure 30: Total building electric bill cost and savings for the three representative weeks for El Paso with PV. Includes thermal and non-thermal load.

In San Diego, adding PV to the No PV scenario alone saves 30% or $41,914 from the total building electric bill cost. Adding TES with MPC saves 9% whether or not there is PV. In Las Vegas, as there is high PV resource and the utility rate is energy dominated, adding PV reduces the total bill by 53% or $27,301. Adding TES with MPC or schedule further reduces the bill by ∼10%. In El Paso, adding PV alone saves 30% or $14,307 and TES with MPC saves an additional ∼15%.

Overall the TES with MPC can save 8-15% on the annual cost relative to baseline. For the MPC, the average savings are 11.7% for no PV and 10.7% for PV. For the schedule, the average savings are ∼8% for both no PV and PV.

References

[1] P. Denholm and M. Hand, "Grid flexibility and storage required to achieve very high penetration of variable renewable electricity," *Energy Policy*, vol. 39, no. 3, pp. 1817–1830, 2011.

[2] A. Odukomaiya, J. Woods, N. James, S. Kaur, K. R. Gluesenkamp, N. Kumar, S. Mumme, R. Jackson, and R. Prasher, "Addressing energy storage needs at lower cost via on-site thermal energy storage in buildings," *Energy Environ. Sci.*, vol. 14, pp. 5315–5329, 2021.

[3] A. Odukomaiya, J. Woods, N. James, S. Kaur, K. R. Gluesenkamp, N. Kumar, S. Mumme, R. Jackson, and R. Prasher, "Correction: Addressing energy storage needs at lower cost via on-site thermal energy storage in buildings," *Energy Environ. Sci.*, vol. 15, pp. 395–395, 2022.

[4] Y. Sun, S. Wang, F. Xiao, and D. Gao, "Peak load shifting control using different cold thermal energy storage facilities in commercial buildings: A review," *Energy Conversion and Management*, vol. 71, pp. 101–114, 2013.

[5] K. H. Drees and J. E. Braun, "Development and evaluation of a rule-based control strategy for ice storage systems," *HVAC&R Research*, vol. 2, no. 4, pp. 312–334, 1996.

[6] I. Al-Aali, A. Narayanaswamy, and V. Modi, "A novel algorithm for optimal equipment scheduling and dispatch of chilled water systems with ice thermal storage," *Energy Build.*, no. 274, 2022.

[7] Q. Chen, W. Wei, and N. Li., "Techno-economic control strategy optimization for water-source heat pump coupled with ice storage district cooling system," *Int. J. Refrig.*, no. 138, 2022.

[8] X. Kang, X. Wang, J. An, and D. Yan, "A novel approach of day-ahead cooling load prediction and optimal control for ice-based thermal energy storage (tes) system in commercial buildings," *Energy and Buildings*, vol. 275, p. 112478, 2022.

[9] N. Luo, T. Hong, H. Li, R. Jia, and W. Weng, "Data analytics and optimization of an ice-based energy storage system for commercial buildings," *Applied Energy*, vol. 204, pp. 459–475, 2017.

[10] D. K. Kairui Hao and J. E. Braun, "Comparing the economic performance of ice storage and batteries for buildings with on-site pv through model predictive control and optimal sizing," *Journal of Building Performance Simulation*, vol. 15, no. 5, pp. 691–715, 2022.

[11] M. Saffari, A. de Gracia, C. Fernández, M. Belusko, D. Boer, and L. F. Cabeza, "Optimized demand side management (dsm) of peak electricity demand by coupling low temperature thermal energy storage (tes) and solar pv," *Applied Energy*, vol. 211, pp. 604–616, 2018.

[12] A. Tam, D. Ziviani, J. E. Braun, and N. Jain, "Development and evaluation of a generalized rule-based control strategy for residential ice storage systems," *Energy and Buildings*, vol. 197, pp. 99–111, 2019.

[13] X. Wang, X. Kang, J. An, H. Chen, and D. Yan, "Reinforcement learning approach for optimal control of ice-based thermal energy storage (tes) systems in commercial buildings," *Energy and Buildings*, vol. 301, p. 113696, 2023.

[14] X. Wang, X. Liu, Y. Wang, X. Kang, R. Geng, A. Li, F. Xiao, C. Zhang, and D. Yan, "Investigating the deviation between prediction accuracy metrics and control performance metrics in the context of an ice-based thermal energy storage system," *Journal of Energy Storage*, vol. 91, p. 112126, 2024.

[15] E. Bonnema, A. Allen, E. Lee, M. S. Mitchell, and R. Meyer, "Flexible integration of diverse HVAC technologies in EnergyPlus via Python-enabled workflows," *ASHRAE Journal*, 4 2024.

[16] J. D. West and J. E. Braun, "Modeling partial charging and discharging of area-constrained ice storage tanks," *Hvac&r Research*, vol. 5, pp. 209–228, 1999.

[17] K. H. Drees and J. E. Braun, "Modeling of area-constrained ice storage tanks," *HVAC&R Research*, vol. 1, no. 2, pp. 143–158, 1995.

[18] F. P. Incropera and D. P. DeWitt, *Fundamentals of Heat and Mass Transfer*. New York City, New York: John Wiley & Sons, 5th ed., 2002.

[19] R. Judkoff and J. Neymark, "International energy agency building energy simulation test (bestest) and diagnostic method," tech. rep., National Renewable Energy Laboratory, 2 1995.

[20] O. of Energy Efficiency and R. Energy, "Prototype building models." Accessed: 2023-12-30.

[21] U.S. Department of Energy, "Electric chiller model based on condenser entering temperature," in *EnergyPlus Version 23.2.0 Documentation: Engineering Reference*, U.S. Department of Energy, 2023.

[22] N. Blair, N. DiOrio, J. Freeman, P. Gilman, S. Janzou, T. Neises, and M. Wagner, "System advisor model (SAM) general description (version 2017.9.5)," *National Renewable Energy Laboratory*, 2018.

[23] OpenEI, "AL-TOU2 Secondary (0-500kW)." `https://apps.openei.org/USURDB/rate/view/62f6ce5b44c9426a6a1f23e5`, 2023. [Online; accessed 26-October-2023].

[24] OpenEI, "ME- OLGS-1-TOU." `https://apps.openei.org/USURDB/rate/view/62c7415d7c7b95456b08d3b7`, 2023. [Online; accessed 26-October-2023].

[25] OpenEI, "General Service Rate - TOU Secondary Voltage." `https://apps.openei.org/USURDB/rate/view/5d41f4205457a31218dc8c3d`, 2023. [Online; accessed 26-October-2023].

[26] D. Guittet, P. Gasper, M. Shirk, M. Mitchell, M. Gilleran, E. Bonnema, K. Smith, P. Mishra, and M. Mann, "Levelized cost of charging of extreme fast charging with stationary LMO/LTO batteries," *Journal of Energy Storage*, 2024.

[27] P. Bonami, L. Biegler, A. Conn, G. Cornuejols, I. Grossmann, C. Laird, J. Lee, A. Lodi, F. Margot, N.Sawaya, and A. Waechter, "An algorithmic framework for convex mixed integer nonlinear programs," *IBM Research Report RC23771*, Oct. 2005.

[28] A. Wächter and L. T. Biegler, "On the implementation of a primal-dual interior point filter line search algorithm for large-scale nonlinear programming," *Mathematical Programming*, no. 106, pp. 25–57, 2006.

[29] W. E. Hart, J.-P. Watson, and D. L. Woodruff., "Pyomo: modeling and solving mathematical programs in python.," *Mathematical Programming Computation*, no. 3, pp. 219–260, 2011.

[30] U.S. Department of Energy, "Chapter 7.5: User-defined component models," in *EnergyPlus Version 23.2.0 Documentation: Application Guide for EMS*, U.S. Department of Energy, 2023.

[31] A. Mahvi, K. P. Shete, A. Odukomaiya, and J. Woods, "Measuring the maximum capacity and thermal resistances in phase-change thermal storage devices," *Journal of Energy Storage*, vol. 55, p. 105514, 2022.